Petrogenesis of the Eocene and Mio–Pliocene alkaline basaltic magmatism in Meseta Chile Chico, southern Patagonia, Chile: Evidence for the participation of two slab windows

Felipe Espinoza[a,*], Diego Morata[a], Ewan Pelleter[b], René C. Maury[b], Manuel Suárez[c], Yves Lagabrielle[d], Mireille Polvé[e,a], Hervé Bellon[b], Joseph Cotten[b], Rita De la Cruz[c], Christelle Guivel[f]

[a]*Departamento de Geología, Universidad de Chile, Casilla 13518, Correo 21, Santiago, Chile*
[b]*UMR 6538 Domaines Océaniques, Université de Bretagne Occidentale, avenue le Gorgeu, C.S. 93837, 29238 Brest Cedex 3, France*
[c]*Servicio Nacional de Geología y Minería, Avda. Santa María 0104, Santiago, Chile*
[d]*UMR 5573 CNRS, Université de Montpellier, Laboratoire de Dynamique de la Lithosphère (LDL), Groupe de Tectonique, Place Eugène Bataillon 34095 Montpellier Cedex 5, France*
[e]*OMP, Université Paul-Sabatier, UMR 5563 CNRS, 38 rue des 36—Ponts-31400 Toulouse, France*
[f]*Université de Nantes, Laboratoire de Planétologie et Geodynamique-Pétrologie Structurale, 2 rue de la Houssinière, B.P. 92208-44322, Nantes Cedex 03, France*

Abstract

The Meseta Chile Chico (MCC, 46.4°S) is the westernmost exposure of Eocene (lower basaltic sequence, LBS; 55–40 Ma, K–Ar ages) and Mio–Pliocene (upper basaltic sequence, UBS; 16–4 Ma, K–Ar ages) flood basalt volcanism in Patagonia. The MCC is located south of the Lago General Carrera-Buenos Aires (LGCBA), southeast from the present day Chile Triple Junction (CTJ), east of the actual volcanic gap between Southern South Volcanic Zone and Austral Volcanic Zone (SSVZ and AVZ, respectively) and just above the inferred location of the South Chile Ridge segment subducted at ~6 Ma (SCR-1). Erupted products consist of mainly ne-normative olivine basalt with minor hy-normative tholeiites basalt, trachybasalt and basanite. MCC lavas are alkaline (42.7–53.1 wt.% SiO_2, 3–8 wt.% Na_2O+K_2O) and relatively primitive (Ni: 133–360 ppm, Cr: 161–193 ppm, Co: 35–72 ppm, 4–16.5 MgO wt.%). They have a marked OIB-like signature, as shown by their isotopic compositions ($^{87}Sr/^{86}Sr_o$=0.70311–0.70414 and εNd=+4.7–+5.1) and their incompatible trace elements ratios (Ba/La=10–20, La/Nb=0.46–1.09, Ce/Pb=15.52–27.5, Sr/La<25), reflecting deep mantle origin. UBS-primitive lavas have characteristics similar to those of the Eocene LBS basalts, while UBS-intermediate lavas show geochemical imprints (La/Nb>1, Sr/La>25, low Ce/Pb, Nb/U) compatible with contamination by arc/slab-derived and/or crustal components. We propose that the genesis and extrusion of

* Corresponding author. Tel.: +56 2 6784112; fax: +56 2 6963050.
E-mail address: feespino@ing.uchile.cl (F. Espinoza).

magmas is related to the opening of two slab windows due to the subduction of two active ridge segments beneath Patagonia during Eocene and Mio–Pliocene.

Keywords: Chilean Patagonia; Alkali basalts; K–Ar ages; Geochemistry; Slab window

1. Introduction

The Cenozoic geodynamic evolution of the western margin of South America has been dominated by the subduction of different lithospheric plates and various oceanic spreading ridges (e.g. Cande and Leslie, 1986). In particular, oblique subduction of the South Chile spreading Ridge (SCR) beneath the South American plate began 14–15 Ma ago when a segment of the ridge collided with the Chile Trench near Tierra del Fuego (~55°S, Cande and Leslie, 1986), generating a triple junction (the Chile Triple Junction, CTJ). Since then, the resulting northward migration of the CTJ implied the subduction of various fracture zone–ridge segments (oriented ~N160), the last of which started subducting ~0.3 Ma ago (SCR1, Cande and Leslie, 1986; Bourgois et al., 2000) at the Taitao Peninsula (46°12′S, Guivel et al., 1999; Fig. 1A and B).

North of the CTJ the convergence between the Nazca and South American plates is now represented by a N80 relative motion with an average rate of 84 mm/year (Gripp and Gordon, 1990; DeMets et al., 1990). South of the CTJ, the present convergence rate of the Antarctic and South American plates is 20 mm/year in an E–W direction (Gripp and Gordon, 1990; DeMets et al., 1990) (Fig. 1B), and the total rate of seafloor spreading at the Chile Ridge is 6 cm/year (Cande and Kent, 1992). This kinematic regime has probably governed the relative motions of the three plates at least since the late Miocene, but the subduction of the Nazca plate below southern South America has experienced different stages since ~26 Ma. During the last stage from ~20 Ma, subduction has been slightly oblique to the Chile Trench axis (Pardo-Casas and Molnar, 1987; Thomson et al., 2001; Cembrano et al., 2002).

According to the paleotectonic reconstructions of Cande and Leslie (1986), another active ridge, the Farallon-Aluk ridge, collided with the western border of South America during Paleocene–Eocene (~55–53? Ma). The triple junction migrated southward, reaching Patagonian latitudes around 50 Ma ago.

The subduction of active, still divergent mid-ocean ridges below continental plates is thought to produce a gap between the two subducting plates under the continental back-arc region (the so-called slab window), which allows decompression melting of upwelling asthenosphere from sub-slab regions (Dickinson and Snyder, 1979; Thorkelson, 1994, 1996) and subsequent generation of mafic plateau volcanism in the back-arc domain. Magmas generated under these conditions are expected to reproduce the chemistry of the asthenospheric mantle beneath the subducting plate (Stern et al., 1990; D'Orazio et al., 2000; Gorring et al., 1997; Gorring and Kay, 2001), although they may suffer contamination during their trip to the surface with consequent modification of their geochemical signature. Many authors have shown that the OIB- and/or MORB-like geochemical signatures of these magmas reflect their deep mantle origin (Dickinson, 1997; Hole et al., 1995; D'Orazio et al., 2000; Benoit et al., 2002). Contamination has been described for some Neogene Patagonian Plateau Lavas (PPL, Gorring et al., 1997; Gorring and Kay, 2001). Some Eocene plateau basalts found in Chilean Patagonia (Demant et al., 1996; Parada et al., 2001) and in the Argentinean Patagonian back-arc region have been interpreted as products of ridge–trench collision (Kay et al., 2002).

The study area, located south of Lago General Carrera-Buenos Aires (LGCBA, 46°30′–47°S, Fig. 1B), is a region where Cenozoic sedimentary and volcanic sequences are well exposed, reflecting the tectonic evolution of western Patagonia. The Meseta Chile Chico (MCC) is located about 300 km east of the Chile Trench, southeast of the actual CTJ, and east of the actual volcanic arc gap between the Southern and Austral Volcanic Zones (SVZ and AVZ, respectively) of the Southern Andes (Fig. 1A and B). This area is characterized by the presence of thick Tertiary flood basalt sequences belonging to a major Patagonian flood basalt province (Patagonian Plateau Lavas). Radiometric ages defined two main basaltic

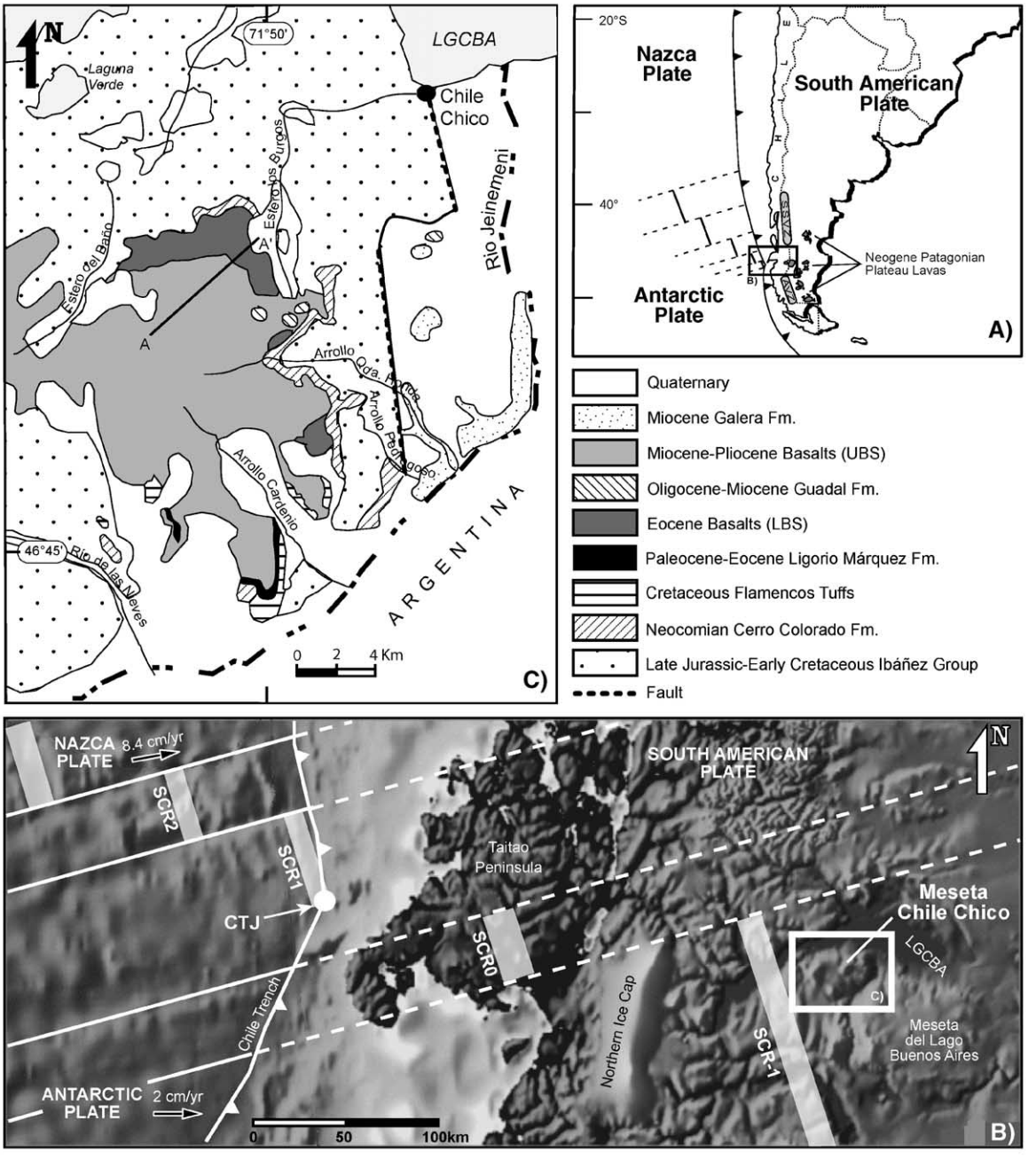

Fig. 1. (A) General view of South America showing approximate location of study area and of Southern South (SSVZ) and Austral Volcanic Zone (AVZ) in the Southern Andes. (B) Tectonic setting of southern South America between 45.8°–47.4°S and 75.8°–76.6°W, in the area of General Carrera-Buenos Aires Lake (LGCBA), showing location of actual Chile Triple Junction (CTJ), Meseta Chile Chico and Meseta del Lago Buenos Aires, relative to fracture zones and southern Chile Ridge (SCR) segments (Cande and Leslie, 1986). Arrows indicate relative sense of motion of Nazca and Antarctic plate with respect to South American plate; numbers are plates average velocity (DeMets et al., 1990). (C) Simplified geological map of the Meseta Chile Chico (46°35′–46°47′S–71°46′–72°02′W), south of General Carrera-Buenos Aires Lake (LGCBA). Line AA′ indicates the position of cross-section in Fig. 2. Modified from Suárez and De la Cruz (2000a).

sequences, in Eocene and Mio–Pliocene times, respectively (Niemeyer, 1975; Charrier et al., 1979; Niemeyer et al., 1984; Petford and Turner, 1996).

The MCC, and a major portion of the Patagonian Plateau Lavas, are located just above the inferred location of the subducted Chile Ridge segment that collided with the South American plate ~6 Ma ago (SCR–1, Fig. 1B). This collision has been demonstrated to produce different major effects at the surface, but most obvious consequence seems to be the extrusion of large volumes of flood basalts (e.g. ~270 km^3 for MCC) in the Patagonian back-arc region (Ramos and Kay, 1992, Stern et al., 1990; Gorring et al., 1997; Gorring and Kay, 2001; Espinoza, 2003; Espinoza and Morata, 2003b).

This paper is focussed on the geochemistry and geochronology of Tertiary volcanic rocks of the MCC, in which Eocene and Mio–Pliocene basaltic sequences are exposed. In this article, new K–Ar ages, geochemical (major and trace elements) and Sr and Nd isotopic data are presented. Details of analytical procedures are given in Appendix A. We construct a geochemical and geodynamic model based on a previous petrogenetic model of Argentinean Patago-

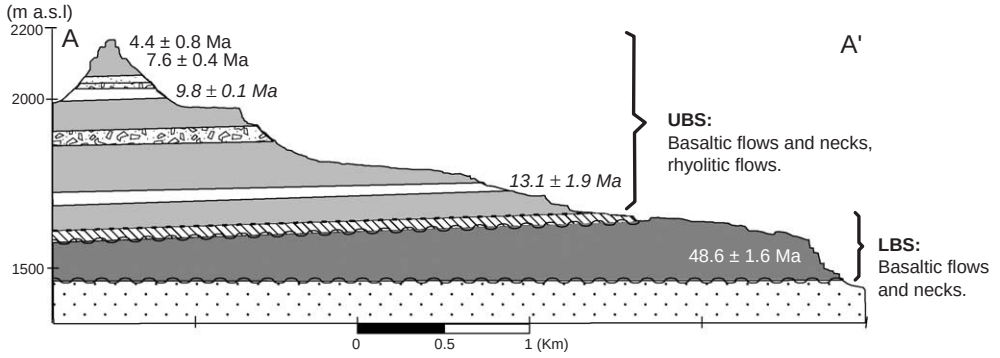

Time	Unit	Origin
Pliocene	Gravels	Fluvial
	UBS Basalts & rhyolites	Volcanic
Miocene	*Galera Fm.*	Fluvial
Oligocene	Guadal Fm.	Marine
	GAP	
Eocene	LBS Basalts	Volcanic
	Ligorio Márquez Fm.	Fluvial
Paleocene	GAP	
Late Cretaceous	calc-alkaline & alkaline magmatism	Volcanic
Early Cretaceous	Flamenco Tuffs	Volcanic
	Cerro Colorado Fm.	Marine
Late Jurassic	Ibáñez Group	Volcanic

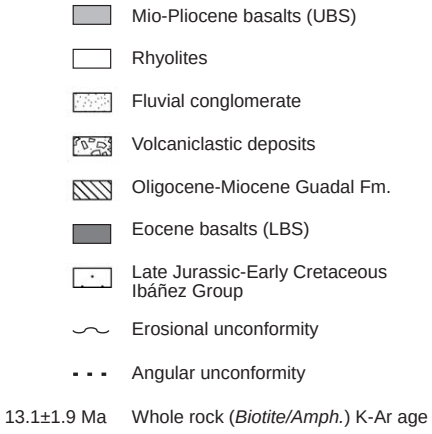

Fig. 2. Meso–Cenozoic lithostratigraphic table and simplified NE–SW geological cross-section through Sombrero hill (see location of section in Fig. 1) for MCC forming sequences. Chronology and stratigraphy of each sequence were taken from literature. Data sources for Tertiary formations are: Ligorio Márquez Fm. (Suárez et al., 2000), Guadal Fm. ("Patagoniano", Frassinetti and Covacevich, 1999; Charrier et al., 1979; Niemeyer et al., 1984), Galera Fm. ("Santacrucense", Marshall and Salinas, 1990; Flynn et al., 2002).

nian Plateau Lavas (Gorring et al., 1997, 2003). in order to demonstrate that the genesis of these magmatic events are related to the opening of two slab windows during the Eocene and the Mio–Pliocene beneath the western margin of South America. A comparison with other Tertiary basaltic sequences and the Patagonian Plateau Lavas is carried out to support this hypothesis.

2. Geological setting

The Mesozoic history of the eastern central Patagonian Cordillera, exposed south of LGCBA, southern Chile, started with the middle Jurassic–early Cretaceous acid subduction-related calc-alkaline volcanic rocks (Baker et al., 1981; Suárez et al., 1999; Suárez and De la Cruz, 2000b) and volcanoclastic deposits of the Ibáñez Group (belonging to the Chon-Aike acid Large Igneous Province; Pankhurst et al., 1998). Over these volcanic rocks, marine sediments with continental interbedding (Neocomian Cerro Colorado Fm., Suárez et al., 2000) were deposited as a consequence of a first stage of a back-arc basin (Austral Basin, Biddle et al., 1986; Riccardi, 1988), and covered by a local subaerial volcanism during early Cretaceous (Barremian Flamencos Tuffs, Suárez et al., 2000; Figs. 1C and 2). The Tertiary record in the Meseta Chile Chico consists of thick sedimentary (marine and continental) successions and subaerial flood basalts (Figs. 1C and 2).

The MCC flood basalts comprise two well defined sequences. The basal lower basaltic sequence (LBS) of the MCC is formed by 500–550 m of Eocene basaltic lava flows and some peridotite xenolith-bearing basanitic necks (57–40 Ma, Charrier et al., 1979; Baker et al., 1981; Petford et al., 1996; Espinoza and Morata, 2003a). This sequence unconformably overlies the Mesozoic Ibáñez Group and the Neocomian

Table 1
Age ranges for Meseta Chile Chico defined sequences

Sequence	Age range [Ma] *Epoch*	No. datations this work (literature)	Principal rock composition
Lower basaltic Sequence (LBS)	55–34 *Eocene*	8 (24)	Basalts
Upper basaltic Sequence (UBS)	16–3 *Mio–Pliocene*	11 (8)	Basalts, rhyolites

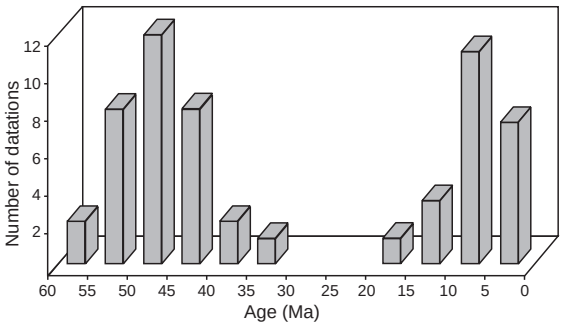

Fig. 3. Histogram showing Meseta Chile Chico K–Ar age distribution (values from this work and compiled data).

Cerro Colorado Formation, at its northern and southern margins, respectively (Fig. 1C). These basalts can be correlated with the 57–45 Ma Posadas Basalt (Baker et al., 1981; Kay et al., 2002) and with the 42±6 Ma Balmaceda Basalts (Baker et al., 1981; Demant et al., 1996), located east and north of the MCC area, respectively.

The present erosion surface of the MCC is flat, and covers about 300 km^2 at an altitude between 1600 and 2200 m above sea level. It corresponds to the 400 m thick upper basaltic sequence (UBS) of Miocene–Pliocene basaltic lava flows and necks (16–3 Ma, Charrier et al., 1979; Espinoza, 2003) (Fig. 1C). At the base of the Miocene basalts and interbedded with them, two rhyolitic flows a few meters thick confer a bimodal character to this sequence (Espinoza, 2003). The Mio–Pliocene basaltic sequence can be correlated with similar volcanic rocks at the Meseta del Lago Buenos Aires (MLBA, Fig. 1B), which is an eastward topographic extension of MCC (the Upper Miocene Meseta Lago Buenos Aires Fm. and the Early Pleistocene El Sello Fm., Busteros and Lapido, 1983; Gorring et al., 2003). According to Espinoza et al. (2003), the UBS would be chronologically, and probably genetically, correlated with the slab window-related Neogene Patagonian Plateau Lavas (Gorring et al., 1997; Gorring and Kay, 2001) exposed to the East in Argentina, and particularly with Mio–Pliocene MLBA lavas (main-plateau lavas of Gorring et al., 2003).

South of LGCBA region, the intrusive activity during Tertiary was restricted to isolated and small late Miocene plutons. The Paso de las Llaves pluton, a satellite body belonging to the eastern part of the North Patagonian Batholith (Pankhurst et al., 1999)

Table 2
Representative EMPA mineral chemistry analysis of Meseta Chile Chico rocks

Mineral	Plagioclase						Pyroxenes					Olivine					Amphibole	Biotite
Sample	FE01-32	FE01-32	FE01-06	FE01-06	FE01-06	FE01-39B	FE01-18	FE01-10	FE01-35	FE01-18	FE01-18	FE01-18	FE01-06	FE01-35	FE01-35	FE01-18	FE01-32	FE01-32
Sequence	UBS	UBS	UBS	UBS	UBS	LBS	UBS	UBS	UBS	UBS	UBS	UBS	UBS	UBS	UBS	UBS	UBS	UBS
Type	Rhyolite	Rhyolite	Basalt	Basalt	Basalt	Basalt	Basalt	Basalt	Basalt	Basalt	Basalt	Basalt	Basalt	Basalt	Basalt	Basalt	Rhyolite	Rhyolite
SiO_2	56.02	62.27	50.27	52.45	55.51	58.49	50.34	46.88	47.33	45.21	43.73	38.50	39.55	36.33	36.32	39.83	45.42	37.02
TiO_2	0.02	0.05	0.09	0.00	0.02	0.24	1.04	2.19	1.60	3.07	3.32	0.02	0.05	0.00	0.00	0.00	1.25	4.10
Al_2O_3	27.93	24.24	31.43	29.48	28.04	26.70	4.22	8.10	8.61	9.85	10.42	0.05	0.17	0.00	0.05	0.03	8.92	14.49
FeO	0.30	0.54	0.87	0.27	0.41	0.57	8.69	6.94	9.16	8.62	7.84	16.60	18.60	36.85	37.01	14.78	15.72	18.08
MnO	0.22	0.00	0.05	0.00	0.00	0.26	0.20	0.13	0.15	0.33	0.00	0.16	0.47	0.72	0.79	0.20	0.84	0.47
MgO	0.00	0.00	0.00	0.00	0.00	0.06	13.21	13.44	13.30	11.96	11.87	44.38	42.61	25.39	24.64	45.49	13.29	13.21
CaO	9.94	5.97	15.62	13.47	11.30	8.45	21.89	22.44	21.33	21.46	21.68	0.19	0.22	0.17	0.29	0.22	11.32	0.10
Na_2O	5.43	7.35	2.82	3.89	5.03	5.45	0.64	0.52	0.40	0.79	0.64	0.00	0.06	0.02	0.03	0.00	1.67	0.47
K_2O	0.24	0.88	0.18	0.40	0.45	0.96	0.00	0.01	0.00	0.00	0.23	0.00	0.00	0.00	0.09	0.00	0.82	8.83
Total	100.09	101.30	101.33	99.96	100.78	101.18	100.24	100.65	101.87	101.29	99.73	99.89	101.72	99.47	99.23	100.54	99.24	96.77
Si	2.518	2.737	2.277	2.388	2.491	2.596	1.877	1.738	1.741	1.679	1.649	0.978	0.993	1.022	1.027	0.994	6.58	2.77
Ti	0.001	0.002	0.003	0.000	0.001	0.008	0.123	0.061	0.044	0.086	0.351	0.000	0.001	0.000	0.000	0.000	0.14	0.23
Al	1.480	1.256	1.678	1.582	1.483	1.397	0.029	0.354	0.373	0.431	0.094	0.001	0.005	0.000	0.002	0.001	1.52	1.27
Fe^{2+}	0.011	0.020	0.033	0.010	0.016	0.021	0.063	0.215	0.282	0.268	0.112	0.353	0.391	0.867	0.875	0.308	1.22	0.73
Fe^{3+}																	0.69	0.40
Mn^{2+}	0.008	0.000	0.002	0.000	0.000	0.010	0.271	0.004	0.005	0.010	0.247	0.003	0.010	0.017	0.019	0.004	0.10	0.03
Mg	0.000	0.000	0.000	0.000	0.000	0.004	0.006	0.743	0.729	0.662	0.000	1.680	1.596	1.065	1.038	1.692	2.87	1.47
Ca	0.479	0.281	0.758	0.657	0.543	0.402	0.734	0.891	0.840	0.854	0.667	0.005	0.006	0.005	0.009	0.006	1.76	0.01
Na	0.473	0.626	0.248	0.343	0.438	0.469	0.875	0.038	0.029	0.057	0.876	0.000	0.003	0.001	0.002	0.000	0.47	0.07
K	0.014	0.049	0.011	0.023	0.026	0.054	0.000	0.001	0.000	0.000	0.011	0.000	0.000	0.000	0.003	0.000	0.15	0.84
Sum	4.984	4.971	5.010	5.004	4.998	4.960	4.024	4.044	4.043	4.048	4.054	3.021	3.005	2.978	2.975	3.006	15.49	7.82

Cation per formula unit of representative plagioclase based on 8O, pyroxenes (6O), olivine (4O), amphibole (23) and biotite (22).

emplaced in the Ibáñez Group 30 km west of the MCC, has rock types ranging from gabbro to granite (Vargas and Hervé, 1995) and K–Ar, Ar–Ar and Rb–Sr ages ranging from 10.3±4 to 9.6±0.5 Ma (Petford and Turner, 1996; Pankhurst et al., 1999; Suárez and De la Cruz, 2001). A neighbouring granitic body in the Avilés river, probably belonging to the Paso de las Llaves pluton, gives a K–Ar age of 9.6±0.6 Ma (Suárez and De la Cruz, 2001).

Recent studies (Ramos and Kay, 1992; Petford et al., 1996, Gorring and Kay, 2001; Gorring et al., 1997, 2003) confirm the ages previously obtained for the Eocene and Mio–Pliocene events in Patagonia, and argue that this magmatism could be related to the opening of slab windows beneath the continent as a consequence of the subduction of active ridges.

3. Geochronology of the MCC volcanic sequences

Several authors (e.g. Charrier et al., 1979; Baker et al., 1981; Niemeyer et al., 1984; Petford and Turner, 1996; Flynn et al., 2002) have reported age determinations from the Meseta Chile Chico basalts (erroneously called the "Meseta Buenos Aires" in some previous papers). For the LBS, most ages are between 55 and 40 Ma (Table 1), with only two younger ages (36±2 Ma and 34.15±0.4 Ma, Charrier et al., 1979; Flynn et al., 2002, respectively). For the UBS, ages mainly range between 12 and 3 Ma (Table 1), with only one older age (16±0.5 Ma, Charrier et al., 1979).

Using all the previously published K–Ar ages together with our 19 new K–Ar ages (16 whole-rock ages and 2 biotite and 1 amphibole separate ages), a clear magmatic gap lasting 24±4 Ma, i.e. between 38±2 and 14±2 Ma (Oligocene to middle Miocene) is defined in this sector of Patagonia during the Tertiary (Fig. 3).

4. Petrography and mineral chemistry

Representative mineral chemistry analyses are listed in Table 2 and displayed in Fig. 4. Olivine, clinopyroxene, plagioclase and minor Fe–Ti oxides are the main phenocrysts in basalts from both sequences. Their textures are intergranular, pilotaxitic, rarely intersertal or ophitic to subophitic (summary of samples petrography in Table 3). Al^{VI}/Al^{IV} in pyroxenes indicates low pressures of crystallization (Simonetti et al., 1996). A major petrographic difference between the two sequences is the presence in the UBS basalts of rounded quartz xenocrysts (1–3 mm) rimmed by clinopyroxene (<0.5 mm wide), the composition of which is similar to those of clinopyroxene phenocrysts of host basalts (Table 3). In general, basalts from UBS are fresher than those from LBS, which contain some secondary minerals (calcite, zeolites and/or mafic phyllosilicates).

5. Geochemistry

5.1. Major and trace element geochemistry

Results of analyses of 40 samples are listed in Table 4.

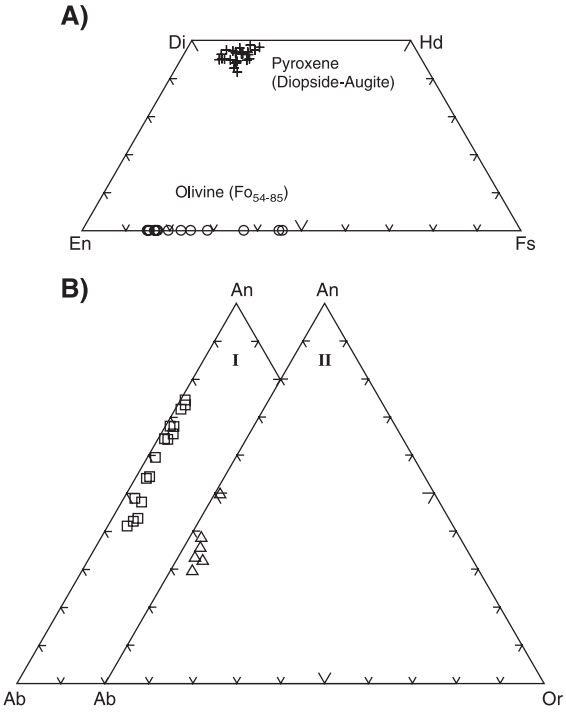

Fig. 4. (A) Classification diagram for pyroxene (Morimoto et al., 1988) and olivine phenocrysts and groundmass crystals from MCC lavas (LBS+UBS). (B) Ab–An–Or compositional triangles for plagioclase phenocrysts and groundmass crystals: (I) MCC mafic lavas (LBS+UBS) and (II) rhyolites from UBS.

Table 3
Summary of petrographic descriptions and observations of Eocene and Mio–Pliocene Meseta Chile Chico volcanic rocks (basalts and rhyolites)

Rock type	Mineral components—phenocrysts	Description	Mineral chemistry	Observations–alterations
Basalts	Olivine (30 to 100 vol.%)	Euhedral/subhedral (0.5–4 mm across), normal zoning	$Fo_{63–85}$ MnO (0.1 to 0.8 wt.%) CaO (0.09 to 0.40 wt.%)	Usually fresh, but incipient alteration (iddingsite, hematite, serpentine+chlorite) along rims and interior cracks
	Clinopyroxene (10 to 90 vol.%)	Euhedral/subhedral (0.4–2 mm in size); fractured, normal zoning and sand-clock twins	$En_{40–46}Fs_{8–15}Wo_{45}$ CaO (21–24 wt.%) TiO_2 (0.6–2.2 wt.%) $En_{41–43}Fs_{11–12}Wo_{48–45}$[a]	Typically fresh Low Al^{VI}/Al^{IV} (0.0–0.8)
	Plagioclase (5 to 20 vol.%)	Euhedral/anhedral (up to 5 mm across); generally twinned, complex zonation patterns	Bytownite–andesine FeO (0.13–1.24 wt.%)	inclusion rings (minerals, glass) and disequilibrium textures (cloudy/sieve-textured)
	Fe–Ti oxides (<5 vol.%)	Usually microphenocrysts	Magnetite and/or illmenite	
	Groundmass	Made up by plagioclase microlites, subordinate clinopyroxene, minor olivine and variable amounts of Fe–Ti oxides	Plg ($An_{64–68}$) Cpx ($En_{37–44}Fs_{13–14}Wo_{43–49}$) Ol ($Fo_{54–75}$) Magnetite and/or illmenite	Partially altered or recrystallized to Cc, Zeo and/or mafic phyllosilicates in fibrous or radial growths, also filling amygdules and thin veins, or in patches in the groundmass as polycrystalline aggregates
Rhyolites	Plagioclase (up to 55 vol.%)	Subhedral with rounded borders (<4 mm across), normal and inverse zonations	$An_{29}Ab_{66}Or_5–An_{50}Ab_{49}Or_1$	Crystals appear isolated or in a cumulated texture alone or with the other phases
	Biotite (up to 30 vol.%) Oriented according to flow direction	Subhedral (up to 4 mm)	Fe-rich intermediate composition (Sideroph-Ann) Ti (0.23–0.25 a.p.f.u.), K (0.72–0.86 a.p.f.u.)	Slightly altered by Cc with occasional Plg inclusions Ti and K contents increasing to the rim
	Amphibole (up to 15 vol.%)	Subhedral (<1.5 mm in size), slightly zoned	Magnesium hornblendes Hi Fe^{3+}, Mg and low Fe^{2+}, Ca contents at the rims	Oriented according to flow direction
	Groundmass	Vitreous texture with tiny plagioclase microlites and magnetite		Oriented Plg microlites

[a] Composition of clinopyroxene rims surrounding quartz xenocrysts in some UBS basalts.

5.1.1. LBS

In the TAS diagram (total alkalis vs. silica diagram, Le Maitre et al., 1989; Fig. 5A) LBS rocks range from basanites to trachybasalts. The rocks are mainly ne-normative olivine basalts with scarce hy-normative olivine tholeiites.

The range of major element compositions and correlations between elements are easily visualized in Fig. 6. The highest concentrations of alkalies (and P_2O_5) are observed in two subvolcanic basanites (e.g. Cerro Lápiz, 4.87 wt.% Na_2O; 2.82 wt.% K_2O). Mg numbers #mg (=molar 100*Mg/(Mg+Fe^{2+}), assuming a Fe^{3+}/Fe^{2+} ratio of 0.15) range from 68 to 77. Negative correlations between MgO and Al_2O_3 and Na_2O are observed (Fig. 6). The high #mg, together with high Ni, Cr and Co contents (up to 360, 415 and 72 ppm, respectively), is typical for primitive mantle-derived melts. The decrease of Ni, Cr and Co with decreasing MgO (Fig. 6) suggests that olivine, clinopyroxene and Cr-spinel played a dominant role during crystal fractionation. High contents of very incompatible elements (e.g. Th and Zr), especially in subvolcanic basanites (Fig. 6), suggest that these magmas were formed by relatively low degrees of partial melting of peridotitic mantle.

On a primitive mantle-normalized diagram (Fig. 7A), lavas from the Eocene LBS show rather smooth patterns lacking major anomalies, with high normalized concentrations of LILE (Ba_N 27–92[78], Rb_N 17–70[85]), HFSE (Th_N 21–62[115], Nb_N 33–83[159], Ti_N 10–14[13]; the values in brackets are from the subvolcanic basanitic neck of Cerro Lápiz) and LREE, similar to the average of oceanic and continental alkali basalts ("OIB", Sun and McDonough, 1989; Thompson et al., 1984). These patterns correspond to those previously found for Eocene MCC lavas (Baker et al., 1981) and for Eocene Posadas Basalt (Ramos and Kay, 1992; Kay et al., 2002; Fig. 7A). The OIB-like signature of LBS rocks is also confirmed by the marked positive correlation between Ba/Nb and La/Nb (Fig. 8), typical of EM-type OIB generated from an enriched mantle (Sun and McDonough, 1989). Other trace element ratios are also similar to those of OIB (Ba/La=10–20, La/Nb=0.66–1.01, La/Nb_{OIB}=0.77; Fig. 8). The Ba/Nb and La/Nb values for LBS are also very similar to those of slab window-related lavas from Antarctic Peninsula (Hole et al., 1995) and Pali-Aike (Stern et al., 1990; D'Orazio et al., 2000).

5.1.2. UBS

UBS rocks are basalt, basanite, trachybasalt, basaltic trachyandesite and rhyolite (Fig. 5B). The basaltic trachyandesites contain quartz xenocrysts and they may therefore be considered as contaminated trachybasalts. Most UBS basalts are alkaline and are mainly ne-and minor hy-normative olivine basalts and tholeiites like the LBS basalts. Rhyolites belong to the high-K calc-alkaline series (Peccerillo and Taylor, 1976). The basic and acid terms of this sequence define a bimodal distribution with a wide silica gap between 54 and 72 wt.% SiO_2 (Fig. 5B.).

Major and trace element compositions and inter-element correlations for UBS basalts are roughly similar to those of LBS (Table 4, Fig. 6), and olivine, clinopyroxene and Cr-spinel must also have played an important role during crystal fractionation. A slightly wider range in concentrations of some highly incompatible immobile elements in the UBS rocks suggests that the degree of partial melting for these magmas varied more than in LBS (Figs. 6 and 9). Two subgroups of UBS basic lavas are recognized on the basis of the TiO_2, Zr vs. MgO (Fig. 6) and Zr/Y vs. FeO_{tot} (Fig. 9) variation diagrams.

Mio–Pliocene UBS basaltic flows and necks display primitive mantle-normalized patterns similar to those from LBS basalts (Fig. 7B), but a wider range of patterns is observed. Compositions in part fall below the field of Plio–Pleistocene MLBA lavas (post-plateau basalts of Gorring et al., 2003, Fig. 7B). The more incompatible element (e.g. Ba, Rb, Th) concentrations scatter near OIB values, reflecting mobility during magma genesis. HFSE patterns are generally subparallel, but some samples show positive Pb anomalies and/or marked negative Nb and Ti anomalies. These differences confirm the presence of the two subgroups identified above (Figs. 6, 7B and 9), which are repeated in the Ba/Nb vs. La/Nb diagram (Fig. 8), where primitive UBS lavas with higher FeO_{tot}, Ti_N (TiO_2) and Nb_N values plot close to the origin (La/Nb 0.46–1.09), together with the LBS rocks, near the La/Nb ratio characteristic for OIB (La/Nb_{OIB} 0.77). Primitive UBS lavas show similarities with slab window-related lavas from

Table 4
Representative geochemical analyses of Eocene and Mio–Pliocene Meseta Chile Chico volcanic rocks

Unit	Lower basaltic sequence (LBS)													
Sp. no.	FE01-39B[a]	FE01-41A	CC-180	CC-267	CC-284	CC-285	PG24	PG26	PG27	PG31	PG53-L	PG55	PG141	PG144
Type	Basanite	Basanite	Basalt	Basalt	Basalt	Basalt	Trachybasalt	Basalt	Basalt	Basanite	Basalt	Basalt	Trachybasalt	Basanite
SiO_2	44.23	44.07	44.21	46.16	45.44	45.19	46.60	45.70	47.00	42.65	44.00	47.00	46.50	43.35
TiO_2	2.83	2.75	2.57	2.74	2.24	2.51	2.78	2.10	2.62	2.83	2.5	2.95	2.06	3.01
Al_2O_3	14.77	14.23	14.61	15.05	13.70	14.50	14.53	13.70	13.65	11.95	13.00	14.30	16.00	13.85
Fe_2O_3	4.64	5.87	3.53	4.05	4.43	3.71	13.34	12.65	13.26	14.58	13.25	13.30	10.10	13.40
FeO	8.58	6.50	7.85	8.16	7.43	8.75								
MnO	0.20	0.20	0.18	0.21	0.18	0.19	0.19	0.17	0.18	0.19	0.19	0.17	0.14	0.19
MgO	6.78	8.01	9.93	7.61	10.84	9.34	7.20	9.30	7.82	13.75	9.6	7.04		
CaO	7.21	7.56	9.67	8.61	8.59	9.11	8.15	7.90	8.10	8.80	9.3	7.65	9.35	8.10
Na_2O	4.87	4.83	2.36	3.29	2.04	2.56	3.58	2.54	3.35	2.48	2.35	3.12	4.20	4.30
K_2O	2.82	1.80	1.45	1.57	0.91	1.17	1.62	1.66	1.41	1.29	1.00	1.22	1.39	2.26
P_2O_5	1.02	1.03	0.50	0.56	0.39	0.48	0.67	0.40	0.66	0.53	0.47	0.53	0.51	0.90
Sum	99.87	99.83	99.54	99.67	99.85	99.53	99.47	100.40	100.04	99.97	99.19	99.77	100.13	99.64
LOI	1.92	2.98	2.68	1.66	3.66	2.02	0.81	4.28	1.99	0.92	3.53	2.49	3.68	1.83
Rb	54.09		29	21	11	15	35	29	45	17	18	20	22	23
Sr	1138.56	1020	682	621	490	938	660	620	575	635	532	505	755	965
Ba	542.18	510	641	334	431	249	375	190	288	300	280	250	323	355
Sc	13.56	12	26	18	25	23	18	23	21	23	24	19	23	18
V	176.38	179	238	182	219	232	200	220	198	260	255	230	206	225
Cr	155.79	255	284	161	263	191	200	280	225	415	290	230	165	293
Co	36.22	42	49	39	45	45	44	53	50	72	56	49	35	48
Ni	145.58	185	182	133	144	173	147	210	180	360	165	185	86	160
Y	29.32	25	25	23	20	21	27	22	26	19	24.5	29	22	25
Zr	419.17	100	212	240	150	186	240	154	245	190	195	240	190	287
Nb	113.48	88	53	37	31	37	38	24	36	44	31.5	37	34	59
Ta	6.95													
Th	9.66	12.0	5.2	3.2	2.5	3.7	3.0	1.8	2.5	2.8	2.5	2.9	3.8	4.1
Cs	0.59													
U	3.21													
Pb	5.44		<4	<4	<4	<4								
Hf	9.25	8.9	7.7	7.4	5.1	6.2								
La	78.79	71.0	37.0	32.0	21.0	26.0	33.5	18.5	29.0	29.0	23.5	26.5	34.0	46.0
Ce	149.63	144.0	81.0	75.0	49.0	63.0	69.0	40.0	58.5	57.0	53.0	55.0	66.0	92.0
Nd	59.17	60.0	38.0	38.0	27.0	32.0	39.0	25.0	34.0	31.0	29.0	32.0	31.0	45.0
Sm	10.39	10.00	7.94	8.07	5.62	6.66	7.70	5.70	6.50	6.30	7.00	6.80	6.30	9.15
Eu	3.36	3.00	2.46	2.65	1.85	2.15	2.47	1.75	2.34	2.04	2.1	2.37	1.88	2.68
Gd	9.44	7.92	7.33	7.40	5.74	6.33	6.80	4.90	6.50	5.60	6.1	7.20	5.60	7.80
Dy	6.51	5.68	5.62	6.11	4.74	4.90	5.50	4.25	5.50	4.20	4.8	5.45	4.30	5.30
Ho	1.20	1.00	0.98	1.04	0.84	0.82								
Er	2.81	2.15	2.10	2.02	1.81	1.71	2.50	1.90	2.45	1.90	2.1	2.70	1.90	2.20
Yb	2.35	2.11	1.90	1.92	1.72	1.61	2.03	1.73	1.92	1.50	1.8	1.97	1.65	1.72
Lu	0.34	0.32	0.22	0.23	0.20	0.21								

FE01—samples analyzed by ICP-AES at University of Chile; CC—samples at the SERNAGEOMIN, Chile; PG—samples at the UBO, Brest, France.

[a] Samples analysed by ICP-MS at the Centro de Instrumentación Científica, Granada, España.

Patagonia and Antarctica (D'Orazio et al., 2000; Hole et al., 1995, respectively). Intermediate UBS lavas with lower FeO_{tot}, Ti_N (TiO_2) and Nb_N values have higher La/Nb ratios (up to 3; Fig. 8). Their La/Nb ratios are closer to those of the Southern South Volcanic Zone lavas, the plutonic rocks of the Patagonian Batholith, the Paleozoic plutonic and metasedimentary rocks of the basement and the Chile

Upper basaltic sequence (UBS)												
FE01-06	FE01-07	FE01-13[a]	FE01-16	FE01-17	FE01-20	FE01-23	FE01-27	FE01-29	FE01-31	FE01-32	FE01-35	FE01-36[a]
Basalt	B. trachyand.	Trachybasalt	Trachybasalt	Tephrite	Basalt	Basalt	Basalt	Rhyolite	Trachybasalt	Rhyolite	B. trachyand.	Basalt
47.02	49.32	47.30	48.50	41.03	51.04	45.38	45.31	68.59	46.18	70.83	53.17	46.01
1.51	1.50	2.30	1.72	2.95	1.50	1.41	2.23	0.26	2.36	0.23	1.50	1.42
15.94	17.50	16.15	18.70	12.30	17.30	16.14	14.20	14.50	16.50	14.75	16.92	14.20
3.96	2.59	7.06	2.66	3.52	3.14	3.36	3.67	0.92	3.71	1.03	3.55	5.73
5.75	6.03	4.18	6.54	10.07	6.12	7.19	8.68	0.79	7.24	0.56	4.27	4.55
0.15	0.15	0.15	0.15	0.17	0.15	0.16	0.16	0.09	0.15	0.09	0.13	0.15
10.58	5.24	6.35	5.09	14.35	5.79	9.74	9.31	0.59	7.52	0.32	4.04	11.41
9.36	8.39	9.11	8.90	9.40	8.98	10.08	9.56	1.87	8.44	1.96	8.89	10.03
3.66	4.12	3.97	3.97	2.48	3.88	3.07	3.12	3.44	3.99	3.80	3.86	2.79
1.13	2.23	1.68	2.12	1.36	1.02	1.39	0.77	4.28	1.81	3.86	1.89	1.29
0.42	0.52	0.62	0.62	0.46	0.29	0.47	0.35	0.04	0.68	4.14	0.45	0.60
99.89	99.78	99.76	99.77	99.97	99.71	99.86	99.75	99.94	99.74	99.83	99.87	99.77
0.41	2.19	0.89	0.80	1.88	0.50	1.47	2.39	4.57	1.16	2.08	1.20	1.59
		28.99										23.50
743	1030	855.98	960	575	550	680	445	410	820	460	676	1020.39
365	478	366.61	510	165	246	332	148	970	393	980	430	390.36
24	23	25.08	20	21	27	27	20	2	19	2	23	27.27
227	200	218.09	200	279	186	233	214	18	194	17	212	209.87
369	80	164.30	28	374	94	350	341	10	242	5	63	459.82
33	25	34.68	26	63	28	34	48	3	40	2	27	46.61
191	45	67.78	21	401	57	164	161	4	139	7	36	320.98
18	22	22.01	21	18	21	24	19	11	19	10	21	22.30
98	45	206.57	28	140	134	76	138	155	184	124	72	163.35
21	12	34.93	32	45	21	18	37	24	49	22	33	16.72
		2.10										0.98
7.3	11.0	4.08	7.8	4.6	5.1	7.9	4.7	30.0	6.0	27.0	11.0	4.89
		0.65										0.64
		1.11										1.12
		4.94										7.09
4.3	5.3	5.09	4.8	5.6	3.7	4.5	4.5	4.2	4.9	3.6	4.7	4.13
24.0	35.0	37.28	35.0	26.0	19.0	26.0	17.0	39.0	32.0	36.0	34.0	34.01
61.0	77.0	76.64	79.0	58.0	40.0	60.0	40.0	69.0	68.0	66.0	60.0	73.53
31.0	36.0	34.68	38.0	28.0	22.0	29.0	23.0	25.0	33.0	22.0	31.0	36.28
5.65	7.04	7.02	7.64	6.27	4.19	6.43	4.60	3.62	6.39	3.53	6.05	7.21
1.65	2.13	2.38	2.38	1.92	1.47	2.07	1.61	0.86	2.04	0.86	1.92	2.29
4.75	6.30	6.41	6.78	6.00	4.68	5.83	4.35	2.80	5.84	2.48	5.23	6.52
4.17	5.17	4.78	5.01	4.63	4.38	5.08	3.97	2.43	4.43	2.41	4.49	4.64
0.73	0.80	0.93	0.90	0.78	0.90	0.96	0.75	0.51	0.77	0.50	0.80	0.89
1.93	1.91	2.18	2.03	1.80	2.36	2.48	1.61	1.37	1.68	1.38	1.76	2.11
1.90	1.95	1.75	2.04	1.80	2.30	2.49	1.60	1.39	1.58	1.34	1.74	2.05
0.28	0.30	0.25	0.31	0.27	0.35	0.39	0.24	0.21	0.24	0.21	0.26	0.30

(continued on next page)

Trench sediments. The two subgroups of UBS lavas probably had different origins. The enrichments observed in LBS and UBS rocks do not vary systematically with age (Table 5).

The three UBS rhyolitic lava flows have very similar primitive mantle-normalized patterns (Fig. 7C), with high LILE concentrations, positive Pb and K anomalies, marked Nb, P and Ti negative anomalies, and low concentrations of the less incompatible elements (HFSE+HREE). The marked P and Ti depletion is probably related to the fractionation of minerals such as apatite and Fe–Ti

Table 4 (*continued*)

Unit	Upper basaltic sequence (UBS)												
Sp. no.	CC-313	CC-317-2	CC-317-3	PG22	PG25	PG33	PG36	PG37	PG38	PG54b	PG56	PG138	PG139
Type	Basalt	B. trachyand.	Rhyolite	Basalt	Trachybasalt	Basanite	Trachybasalt	Trachybasalt	Basanite	Basalt	Basalt	Basalt	Basalt
SiO_2	48.00	52.00	69.51	47.10	43.85	43.00	46.70	50.00	42.90	48.00	44.80	48.10	47.00
TiO_2	1.33	1.52	0.24	1.08	2.66	2.22	2.75	1.68	2.77	1.38	2.52	1.40	1.43
Al_2O_3	14.31	18.19	14.85	16.45	14.15	11.25	14.65	17.20	12.00	16.85	13.50	17.25	17.80
Fe_2O_3	5.00	3.64	0.86	9.32	12.46	12.42	13.20	10.60	13.32	9.32	12.90	9.30	8.36
FeO	5.14	4.64	0.54										
MnO	0.17	0.14	0.09	0.28	0.20	0.18	0.18	0.16	0.18	0.16	0.18	0.16	0.17
MgO	11.29	4.38	0.43	7.05	8.72	15.9	7.10	5.25	12.72	7.90	8.80	7.92	5.70
CaO	9.82	8.74	1.87	9.45	9.24	8.8	8.26	9.25	9.83	9.70	8.60	9.60	9.80
Na_2O	2.70	3.72	3.50	2.47	3.36	2.27	3.71	4.02	2.90	3.78	3.70	3.74	3.28
K_2O	0.97	1.99	4.42	2.17	1.59	0.88	1.62	1.50	0.90	0.97	0.97	1.01	0.97
P_2O_5	0.52	0.43	0.07	0.52	0.60	0.58	0.65	0.44	0.47	0.61	0.50	0.60	0.63
Sum	99.63	99.84	99.86	99.68	99.5	100.10	99.23	99.77	99.73	99.07	99.32	99.33	100.01
LOI	0.38	0.45	3.48	3.79	2.67	2.60	0.41	−0.33	1.74	0.40	2.85	0.25	4.87
Rb	29	50	151	69	20	14	29	34	13	19	16	20	17
Sr	769	694	424	645	780	595	680	680	615	1000	500	1100	1080
Ba	431	1230	962	1220	420	430	370	410	195	435	560	430	547
Sc	30	25	2	38	21	23	20	23	26	22	27	21	21
V	235	206	14	285	235	225	205	210	280	232	260	218	217
Cr	671	60	<5	230	285	385	205	76	440	232	350	213	130
Co	40	22	2	37	49	70	46	32	65	35	53	33	22
Ni	294	24	<2	102	190	610	145	33	345	140	205	131	44
Y	19	22	12	23	25	21	28	26	20	23	27	23	24
Zr	113	149	150	115	310	182	250	156	182	162	225	158	164
Nb	17	19	18	7	71	57	41	15	37	13	38	14	14
Ta													
Th	4.5	7.5	18.0	4.9	5.5	4.2	2.8	3.3	2.2	3.1	3.2	3.3	3.1
Cs													
U													
Pb	<4	6.00	16.00										
Hf	4.5	5.0	4.4										
La	29.0	26.0	38.0	25.0	50.0	37.0	33.0	27.0	26.5	29.0	28.0	30.5	32.5
Ce	61.0	59.0	69.0	50.0	94.0	66.0	64.0	56.0	52.0	62.0	63.0	66.0	72.0
Nd	29.0	29.0	22.0	30.5	41.0	34.0	36.0	30.0	29.5	37.0	34.0	37.0	41.0
Sm	5.45	5.78	3.31	6.70	7.90	6.50	7.80	6.15	6.00	7.00	6.80	7.00	7.40
Eu	1.80	1.70	0.84	1.88	2.49	2.05	2.46	1.94	1.92	2.00	2.20	2.05	2.16
Gd	5.00	5.15	2.26	5.30	6.60	5.70	6.55	5.70	4.90	5.90	6.50	5.60	6.00
Dy	4.00	5.57	2.24	4.40	5.10	4.30	5.40	4.75	4.10	4.10	5.20	4.25	4.35
Ho	0.75	0.89	0.48										
Er	1.84	2.17	1.36	2.15	2.4	2.00	2.50	2.60	1.90	2.00	2.40	2.00	2.20
Yb	1.74	2.09	1.40	2.20	1.90	1.60	1.93	2.11	1.45	1.90	1.95	1.95	2.02
Lu	0.25	0.29	0.22										

oxides. The compositions of UBS rhyolites and the Patagonian Batholith (PB I-type, Kilian and Behrmann, 2003) are very similar (Fig. 7), but some differences between them and the coeval Paso de las Llaves granite (Pankhurst et al., 1999) are seen.

5.2. Rare earth elements

5.2.1. LBS and UBS

Chondrite-normalized rare earth element (REE) patterns for LBS and both groups of UBS basalts are

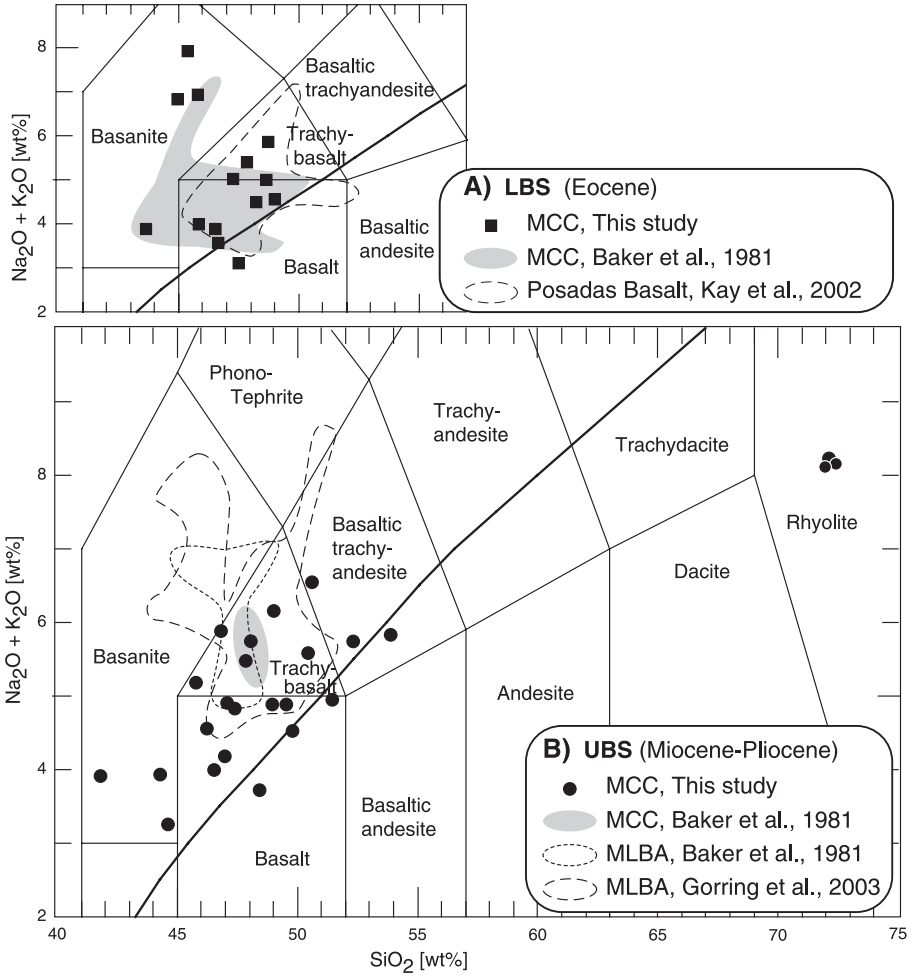

Fig. 5. Total alkali vs. silica classification diagrams (TAS, Le Maitre et al., 1989) and boundary line between alkaline and subalkaline rocks (Irvine and Baragar, 1971) for (A) Eocene MCC rocks (filled squares). Also plotted data from literature: other Eocene MCC lavas (gray field: Baker et al., 1981) and Eocene Posadas Basalt (dashed line: Kay et al., 2002); and (B) Mio–Pliocene Meseta Chile Chico rocks (filled circles). Also plotted data from literature: other Miocene MCC lavas (gray field: Baker et al., 1981) and Plio–Pleistocene MLBA lavas (dotted line: Baker et al., 1981; dashed line: Gorring et al., 2003).

very similar, with high LREE/HREE ratios and no major Eu anomalies (Fig. 10A). LBS lavas have slightly more depleted HREE than UBS samples, and UBS-intermediate lavas have lower Eu values and higher HREE than UBS-primitive rocks (Fig. 10A). High LREE/HREE ratios are typical of OIB-type and intraplate alkali basalts (Sun and McDonough, 1989; Wittke and Mack, 1993). For LBS, the most enriched samples are basanites from necks crosscutting the lava flow sequence.

UBS rhyolites have smooth steep patterns with high LREE enrichments (within the range of UBS basalts), fractionated middle REE, slightly negative Eu anomalies (Eu/Eu*=0.79–0.89) and HREE depletion, below the range of UBS basalts (Fig. 10A).

5.3. Rb/Sr and Sm/Nd isotopes

Three basalt and one rhyolite samples were analysed for Sr and Nd isotopes.

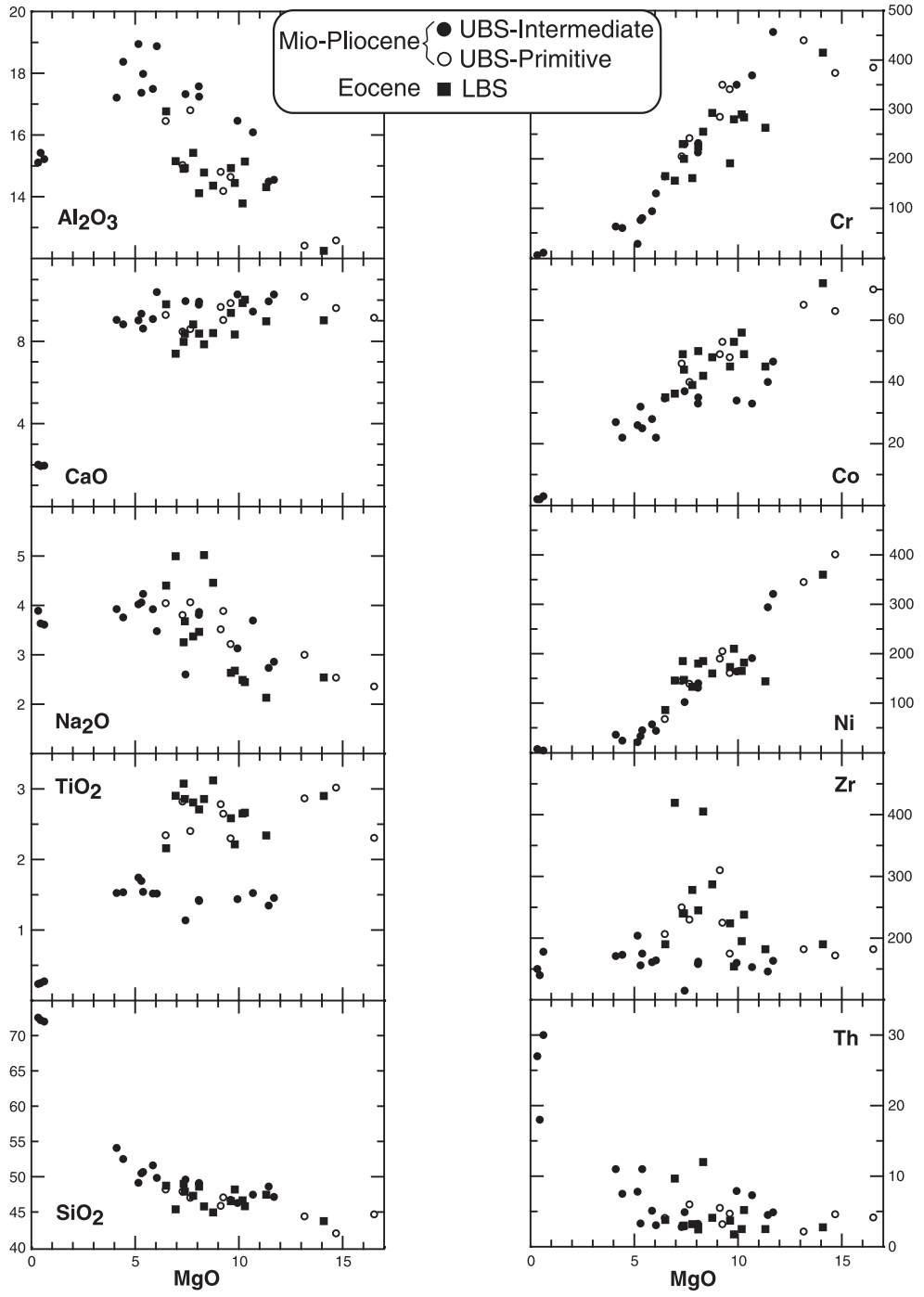

Fig. 6. Variation diagrams of selected major (wt.%) and trace elements (ppm) vs. MgO for Eocene (filled squares) and Mio–Pliocene (open circle: UBS-primitive, filled circles: UBS-intermediate) Meseta Chile Chico rocks. Major elements recalculated on an anhydrous basis. See text for definitions.

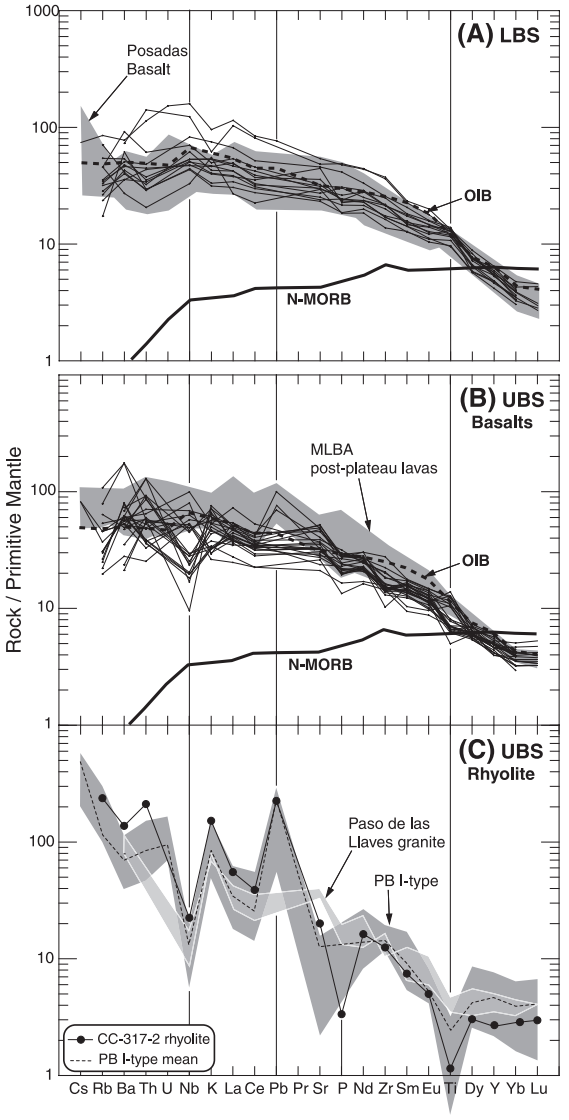

Fig. 7. Primitive mantle-normalized trace element patterns for (A) Eocene (LBS) Meseta Chile Chico rocks (fine solid lines) compared with Eocene Posadas basalt (grey field, Kay et al., 2002); (B) Mio–Pliocene (UBS) Meseta Chile Chico basic rocks (fine solid lines) compared with Plio–Pleistocene MLBA post-plateau lavas (grey field, Gorring et al., 2003); and (C) representative Miocene UBS rhyolitic flow (CC-317-2) compared with coeval Paso de las Llaves granite (light gray field—no Th, Pb and P data; Pankhurst et al., 1999) and PB-I type rocks (Patagonian Batholith plutonic rocks, Kilian and Behrmann, 2003). Typical OIB (dark heavy dashed line), N-MORB (heavy solid line) and normalization factors were taken from Sun and McDonough (1989).

5.3.1. LBS

A representative LBS lava sample (CC-285) has a $(^{87}Sr/^{86}Sr)_o$ ratio of 0.70385 and an εNd value of +5.1, while a basanite (FE01-39B: Cerro Lápiz) displays a $(^{87}Sr/^{86}Sr)_o$ ratio of 0.70311 and a similar εNd value of+4.9 (Table 6). These data are only partly concordant with previous results for MCC (Baker et al., 1981) and Balmaceda (Parada et al., 2001; Hawkesworth et al., 1979) lavas because one MCC and one Balmaceda sample (Hawkesworth et al., 1979) have higher εNd values (+7.0 and +7.4, respectively; Fig. 11). LBS have $(^{87}Sr/^{86}Sr)_o$ and εNd values similar to coeval Posadas Basalts (Ramos and Kay, 1992; Kay et al., 2002), while Paleocene lavas from the base of Posadas Basalt (Ramos and Kay, 1992) have slightly more radiogenic Sr and less radiogenic Nd (Fig. 11).

5.3.2. UBS

The first Sr–Nd isotopic data obtained for UBS lava samples are those for a basalt from the intermediate UBS-subgroup (FE01-36, 4.4±0.8 Ma) and a rhyolite (FE01-29, Table 5). They display $(^{87}Sr/^{86}Sr)_o$ ratios of 0.70414 and 0.70449 and εNd values of +4.7 and +0.7, respectively (Table 6). Likewise LBS lavas, compositions fall in the mantle array (Fig. 11).

The intermediate UBS basalt has similar $(^{87}Sr/^{86}Sr)_o$ ratio but higher εNd value than most Neogene Patagonian Plateau Lavas (Gorring et al., 1997; Gorring and Kay, 2001; MLBA post-plateau basalts of Gorring et al., 2003), with the exception of Pali-Aike lavas (Stern et al., 1990; D'Orazio et al., 2000, 2001), which have the lowest Sr_o and the highest εNd, similar to our UBS sample (Fig. 11). The UBS rhyolite has Sr_o and εNd values very similar to those of the Paso de las Llaves granite (Pankhurst et al., 1999; Fig. 11), and plots within the field of Patagonian Batholith rocks (Pankhurst et al., 1999).

6. Discussion

6.1. Origin of basaltic magmas: REE modelling of partial melting

Ratios between highly incompatible elements can be used to trace petrogenetic processes such as

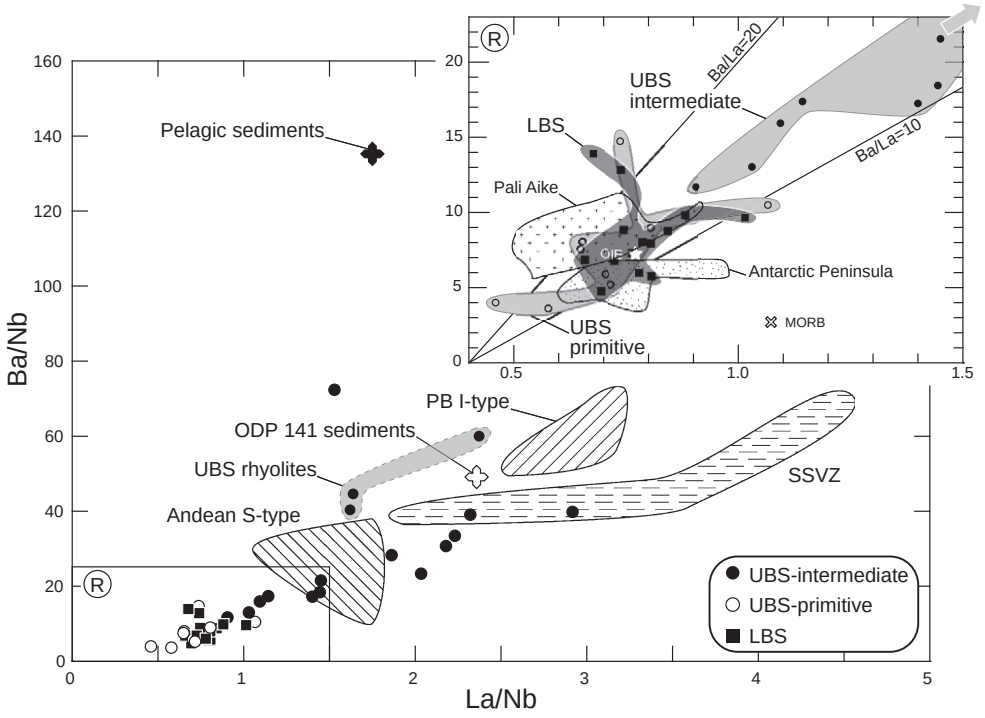

Fig. 8. Plot of Ba/Nb vs. La/Nb for MCC rocks (LBS+UBS) showing strong OIB signature and low LILE/HFSE and LREE/HFSE ratios for LBS (filled squares) and UBS-primitive (open circles) basalts, and slightly higher values for UBS-intermediate (filled circles) samples, compared with mean composition rocks from Southern South Volcanic Zone (SSVZ), Andean S-type (Paleozoic plutonic and metasedimentary rocks), PB I-type crust (plutonic rocks of Patagonian Batholith) and sediments from Chile Trench (ODP 141) and Nazca Plate pelagic sediments (Kilian and Behrmann, 2003). Data of slab window-related lavas from Pali-Aike are also plotted (small crosses, Stern et al., 1990; D'Orazio et al., 2000) and Antarctic Peninsula (fine stipple, Hole et al., 1995).

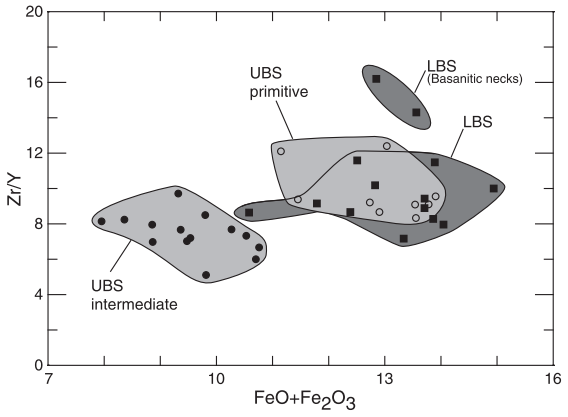

Fig. 9. Plot of Zr/Y vs. Fe_{tot} (Fe_2O_3+FeO wt.%) for MCC basic rocks (LBS+UBS). Note the similarity between LBS and UBS-primitive samples, and their clear differentiation with UBS-intermediate rocks. Also note the higher Zr/Y ratio of LBS basanitic necks.

partial melting or fractional crystallization. For example, the Zr/Y ratio is not significantly affected by fractional crystallization in basaltic systems, but varies only during partial melting (Nicholson and Latin, 1992). As Zr is more incompatible in mantle phases than Y, Zr/Y ratios tend to be higher when the degree of melting is small. Differences in the iron content of the rocks could be related to differences in the depth and/or mantle source composition (Nicholson and Latin, 1992). Thus, high Fe contents and high Zr/Y could indicate high pressures and/or low rates of partial melting during magma generation. Fig. 9 shows that most of LBS and all primitive UBS rocks have Zr/Y ratios between 7 and 12 and very similar Fe_{tot} contents (11–15 wt.% Fe_{tot}). LBS basanites have higher Zr/Y ratios. These features suggest that while LBS and primitive UBS basalts were generated at

Table 5
K–Ar ages of Eocene and Mio–Pliocene Meseta Chile Chico volcanic rocks

Sample	Rock type	Sequence	Dated material	K_2O (wt.%)	$^{40}Ar^*$ ($\times10^{-7}$ cm^3/g)	$^{40}Ar^*$ (%)	Age (Ma)±error (2ó)
FE01-36	Basalt	UBS-Int.	Whole rock	0.987	1.680	89.0	4.40±0.80
PG-138	Basalt	UBS-Int.	Whole rock	0.960	1.383	19.9	4.46±0.44
FE01-11	Basalt	UBS-?	Whole rock	1.743	3.080	73.0	4.50±0.30
FE01-16	Basalt	UBS-Prim.	Whole rock	1.593	2.080	44.0	4.60±0.20
PG 37	Basaltic neck	UBS-Int.	Whole rock	1.420	2.123	42.7	4.63±0.26
CC-317-2	Basalt	UBS-Int.	Whole rock	1.573	4.680	58.0	7.60±0.40
FE01-23	Basaltic neck	UBS-Int.	Whole rock	1.133	3.480	59.0	7.90±0.40
CC-313	Basalt	UBS-Int.	Whole rock	1.330	4.260	28.0	8.20±0.50
CC-317-3	Rhyolite	UBS	Biotite	6.208	23.690	82.0	9.80±0.10
FE01-29	Rhyolite	UBS	Biotite (alt.)	5.905	21.370	79.0	9.30±0.90
FE01-29	Rhyolite	UBS	Hornblende	0.862	4.390	87.0	13.10±1.90
FE01-39B	Basanitic neck	LBS	Whole rock	2.184	34.930	24.0	40.70±1.40
PG 31	Basalt	LBS	Whole rock	1.560	21.860	83.3	42.80±2.00
PG 24	Basaltic neck	LBS	Whole rock	1.680	23.850	84.2	43.50±2.00
CC-267	Basalt	LBS	Whole rock	1.207	21.700	13.0	45.70±1.50
CC-47	Basalt	LBS	Whole rock	0.759	13.910	26.0	46.50±1.70
CC-285	Basalt	LBS	Whole rock	0.815	15.610	15.0	48.60±1.60
PG 55	Basalt	LBS	Whole rock	1.420	22.990	65.4	49.50±2.40
CC-180	Basalt	LBS	Whole rock	1.141	24.030	26.0	53.40±1.80

Decay constant: $\lambda_Z=0.581\times10^{-10}$ $year^{-1}$; $\lambda_\beta=4.96\times10^{-10}$ $year^{-1}$; $^{40}K/K_{total}=0.0167$.
FE01 and CC—samples analysed in the Geochronology Laboratory at the SERNAGEOMIN, Chile.
PG—samples analyzed in the Geochronology Laboratory at the University of Bretagne Occidentale, France.
UBS-Prim.: UBS-primitive lava.
UBS-Int.: UBS-intermediate lava.

fairly similar pressures by equivalent degrees of partial melting from similar mantle sources, the LBS basanites would have a quite different source and form through lower degrees of partial melting. Iintermediate UBS magmas were formed at a different depth and/or from a different mantle source and by slightly higher degrees of partial melting.

HREE contents of LBS and UBS basalts (Yb_N 6.6–9.5) indicate that garnet was present as a residual phase in the mantle sources. To test this hypothesis, the classic, non-modal batch melting equations of Shaw (1970) were used to model the REE patterns of MCC lavas with K_D values from Gorring and Kay (2001). The results can be directly compared with those calculated for MLBA lavas (Gorring et al., 2003). Modelling parameters, mantle sources composition, melt and source mineralogy and mode, and the degree of partial melting are listed in Table 7.

Partial melting of mantle sources between 1% and 4–5% containing 5–9 wt.% of garnet and having slightly different modes could account for the REE concentrations of the more enriched and depleted basalts from UBS (Table 7, Fig. 10C). The more LREE depleted and HREE enriched UBS necks can be modelled by a somewhat higher degree of melting (2–8%) from a slightly different source with less garnet (~5 wt.%). Calculations for LBS lavas indicate that, if their source is grossly similar to the UBS source, it would have to be HREE-depleted to account for the low concentrations of these elements (Table 7, Fig. 10B). Their enriched and depleted concentrations are reproduced by 1% to 4% melting of a mantle source containing 5.5–8 wt.% garnet, but with slightly different source modes for other elements (Table 7, Fig. 10B).

Even the lowest degrees of melting of the LBS lavas source do not generate enriched liquids corresponding to the compositions of the basanites, and thus a more enriched source must be considered in order to reproduce the high incompatible elements concentrations of these necks. McKenzie and O'Nions (1995) have used a metasomatically enriched MORB source to account for the trace element compositions

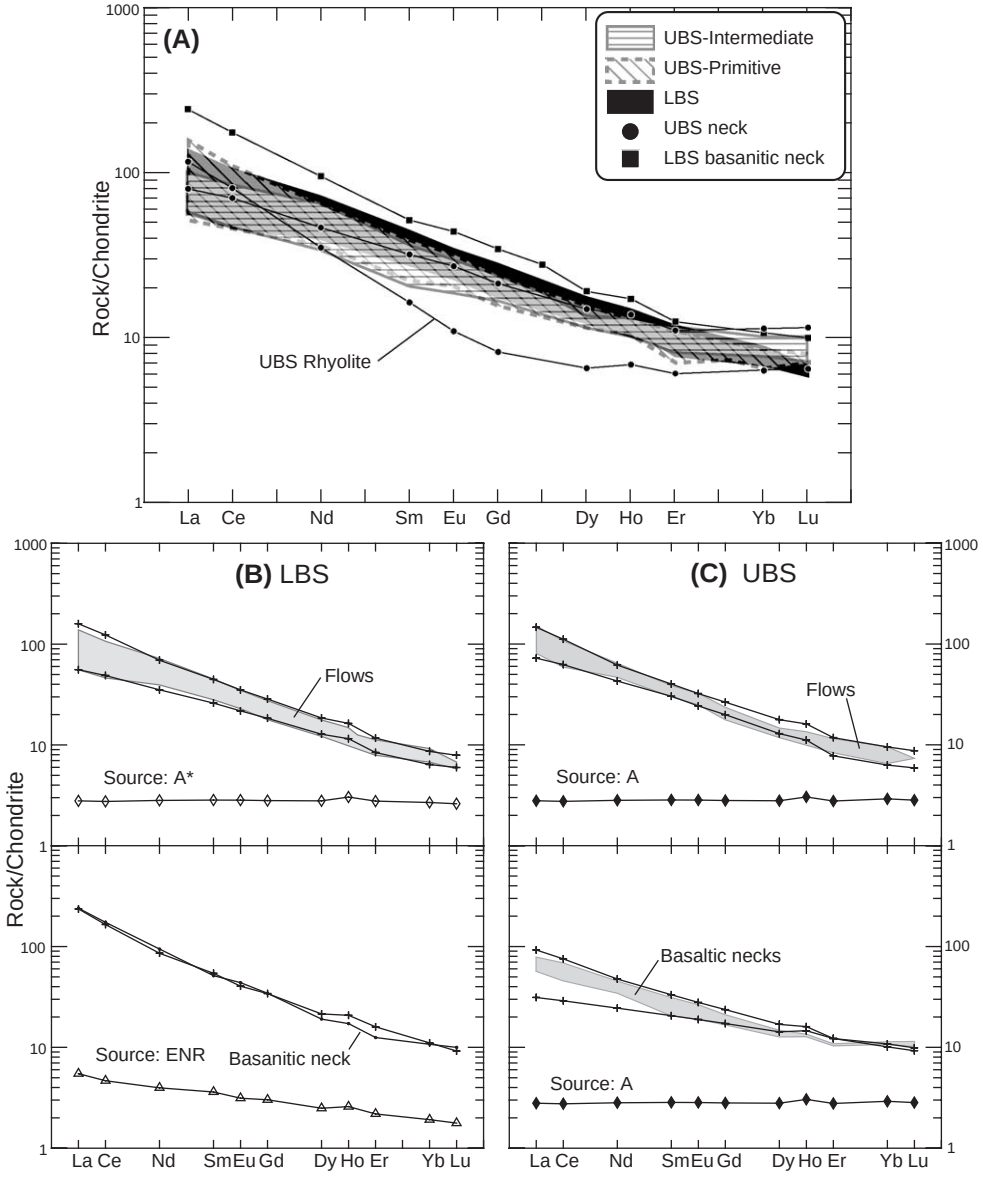

Fig. 10. (A) Chondrite-normalized REE fields and patterns for MCC lavas and necks (plus representative rhyolite), respectively. Below, chondrite-normalized REE patterns of non-modal batch melting models used to approach the MCC rocks compositions (gray fields). (B) Calculated partial melts for LBS lavas and necks (patterns with crosses), and (C) calculated partial melts for UBS lavas and necks (patterns with crosses). Normalizing values are from Nakamura (1974). See Table 7 for model parameters and text for discussion.

of seamount magmas that cannot be modelled by partial melting of either MORB or primitive mantle source. Using this source, the best fit was achieved by 1.5% melting of a MORB source enriched with 8% of a metasomatic fluid (Table 7, Fig. 10B). This fluid has to be highly enriched in incompatible elements and is formed by the extraction of 0.3% melt from the MORB source in the garnet stability field. The results

Table 6
Sr–Nd isotopic data for Eocene and Mio–Pliocene Meseta Chile Chico volcanic rocks and compiled isotopic data from literature

Sample	Rock type	Age (Ma±2σ)	Sequence	Rb	Sr	Sm	Nd	$^{87}Rb/^{86}Sr$	$^{87}Sr/^{86}Sr$	$(^{87}Sr/^{86}Sr)_o$	$^{147}Sm/^{144}Nd$	$^{143}Nd/^{144}Nd$	$(^{143}Nd/^{144}Nd)_o$	εNd_{CHUR}
FE01-36	Basalt	4.4±0.8	UBS-Interm.	22.8	959.0	7.34	36.06	0.06864	0.70414	0.70414	0.123097	0.512877	0.512873	+4.7
FE01-29	Rhyolite	13.1±1.9	UBS	149.7	360.7	2.66	17.10	1.20059	0.70472	0.70449	0.094090	0.512665	0.512657	+0.7
FE01-39B	Basanitic neck	40.7±1.4	LBS	54.1	1138.6	10.39	59.17	0.13741	0.70319	0.70311	0.106175	0.512865	0.512837	+4.9
CC-285	Basalt	48.6±1.6	LBS	14.7	917.2	6.73	29.89	0.04641	0.70388	0.70385	0.136264	0.512878	0.512835	+5.1
P69[a]	Basalt	52	LBS	7.0	294.0	3.93	15.60	0.06887	0.70353	0.70348	0.152388	0.51298	0.512928	+7.0
P71[a]	Basalt	54	LBS	18.0	626.0	8.78	40.50	0.08317	0.70394	0.70388	0.131136	0.51291	0.512864	+5.8
IBA6[b]	Granodiorite	10±0.4	Pat. bath.	73	849	6.36	32.248	0.24900	0.704783	0.70475	0.1192	0.512704	0.512696	+1.4

[a] Baker et al. (1981), MCC basalts.
[b] Pankhurst et al. (1999), Paso de las Llaves granite.

of this model are consistent with the patterns of highly incompatible elements in Eocene MCC lavas as discussed above (Fig. 9).

In conclusion, small degrees of partial melting of a garnet-bearing lherzolitic mantle source are required to explain the REE patterns found in the Tertiary MCC basaltic lavas. The subvolcanic bodies and intrusions that cut each basaltic lava flow sequence display distinctive enrichment patterns and can be modelled in the case of UBS by higher degrees of melting of the same source, and in the case of the LBS necks, by lower degrees of melting of a metasomatically enriched MORB source type mantle. The systematic presence of garnet as a residual phase indicates a depth of melting of 60–75 km, close to the spinel-garnet transition zone, depending on mantle temperature.

6.2. Origin of Miocene rhyolites

The similarities between Miocene UBS rhyolite trace element patterns and isotopic compositions and those of the neighbouring (and coeval) Paso de las Llaves granite (Figs. 7C and 11) suggest that they are genetically related. The origin of the youngest isotopically evolved intrusive rocks of the Patagonian Batholith (late Miocene–Pliocene) is thought to be simultaneous melting of an enriched source, such as the unexposed crystalline lower crust, and mixing with melts from basaltic rocks (underplated subduction-related primary magmas, Pankhurst et al., 1999). Although the isotopic signatures of UBS rhyolites are quite different from those of Jurassic to Cenozoic plutonic rocks from the Patagonian Batholith (Kilian and Behrmann, 2003, Fig. 11, curve D), their trace element patterns are similar (Fig. 7C), and their Sr/La ratios are equivalent to those of Patagonian upper crust values (Fig. 12B). Therefore, the basal rhyolites of the MCC could represent isolated pulses of anatectic magmas which were erupted from a crustal magma chamber after minor crystal fractionation, as shown by their low phenocryst content and vitrophyric textures, together with their negative Ti and P anomalies (Fig. 7C).

6.3. Role of Patagonian crust in UBS petrogenesis

As previously shown, Mio–Pliocene UBS lavas are represented by the primitive UBS subgroup,

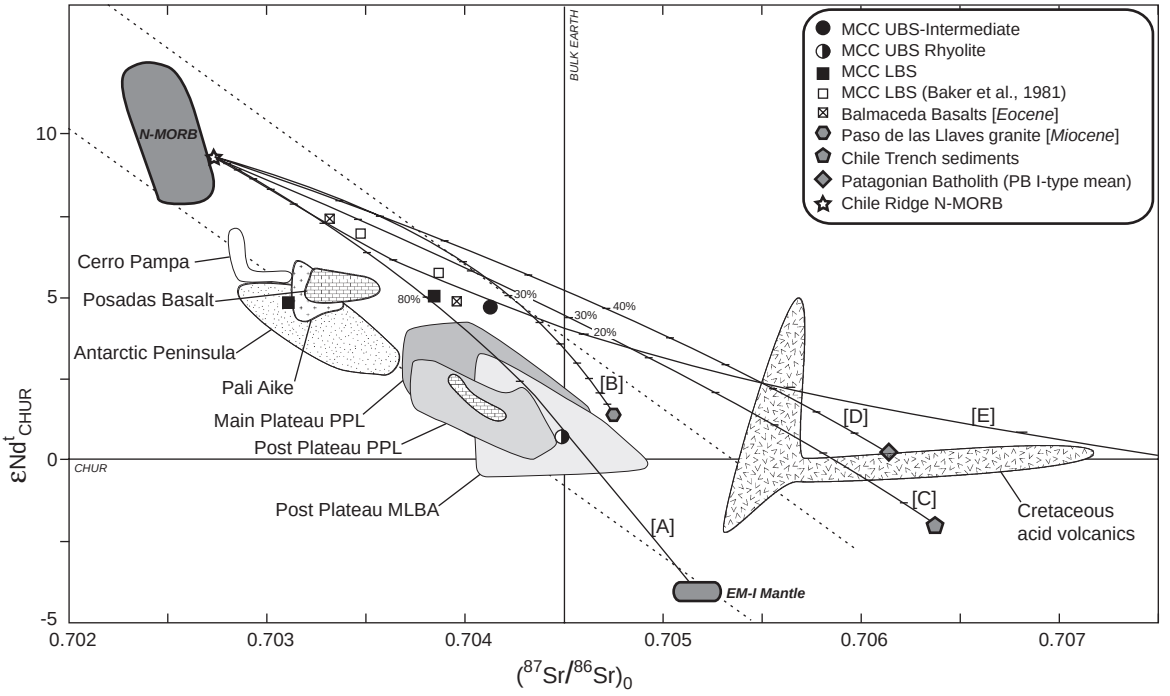

Fig. 11. Initial $^{87}Sr/^{86}Sr$ vs. εNd signatures for Eocene and Mio–Pliocene MCC rocks in the LGCBA area. Black filled squares: LBS basalt (CC-285) and basanitic neck (FE01-39B); black open squares: Eocene MCC lavas from Baker et al. (1981); black filled circle: UBS-intermediate basalt (FE01-36); half black filled circle: Miocene UBS rhyolite (FE01-29). Also plotted data from literature: Brick pattern: Paleocene–Eocene Posadas Basalt (Baker et al., 1981; Ramos and Kay, 1992); V pattern: Cretaceous Patagonian acid volcanics (Parada et al., 2001). Other Tertiary slab window-related lavas from Antarctic Peninsula (Hole et al., 1995), Pali-Aike (Stern et al., 1990; D'Orazio et al., 2000, 2001), Neogene (main- and post-plateau) Patagonian Plateau Lavas (Gorring and Kay, 2001) and post-plateau MLBA lavas (Gorring et al., 2003) are also plotted. Adakites from Cerro Pampa (Kay et al., 1993) are also plotted. Mixing models between basalts from the CTJ N-MORB (CTJ29-3, Guivel et al., 2003) and enriched mantle EM-I (Zindler and Hart, 1986, curve A), Miocene Paso de las Llaves granite (Pankhurst et al., 1999, curve B), sediments from Chilean Trench (CTJ11-10, Guivel et al., 2003, curve C), Patagonian Batholith mean composition (PB I-type, Kilian and Behrmann, 2003, curve D) and Ibáñez Rhyolite (Parada et al., 2001, curve E) are plotted (tick every 10%).

similar to other slab window-related lavas (Figs. 7, 8 and 11), and with a minor, if any, crustal contamination (Figs. 7, 8 and 12), and the intermediate UBS subgroup", also with a typical OIB signature, but with additional components with slab/arc-derived and/or crustal origins.

Elements such as Ba, Pb, Rb, U and Sr are easily mobilised by hydrous fluids generated in subducted MORB or ocean sediments (Hawkesworth et al., 1997), while Th, Nb, Ti and HREE are not soluble in these fluids (Ayers et al., 1997). The HFSE, Nb, Ta and Ti are commonly partitioned into partial melts from asthenospheric sources (Niu and Hékinian, 1997), and Th and LREE are predominantly partitioned into partial melts from the subducted slab (La Tourrette et al., 1993; Stern and Kilian, 1996). High Ba/La, Sr/La and low Ce/Pb ratios characterize fluid-dominated subduction components, whereas high Th/Nb and La/Nb are typical of slab-melt contributions (Elliot et al., 1997; Hawkesworth et al., 1997). The relatively high SiO_2 concentrations for most UBS basalts (46–54 wt.%), together with high La/Nb, low Nb/U, Ce/Pb and Rb/Cs ratios for a representative intermediate UBS lava, compared to a primitive UBS lava and a LBS basanite, indicate either some degree of contamination by a crustal component or source contamination by subducted crustal materials. Furthermore, the intermediate UBS sample fits on the mixing curve between N-MORB and Patagonian Batholith compositions, with less than 10% contamination from the latter component (Fig. 12A).

Table 7
Model parameters and results of non modal batch partial melting calculations (ppm) using various mineralogical and chemical composition for diverse sources to match every rock type described in the text

Phase	Source mode						Melt mode		
	a	a1	b	c	c1	d	a	b	c
Olivine	0.55	0.54	0.55	0.565	0.52	0.57	0.15	0.15	0.1
Opx	0.22	0.21	0.21	0.240	0.21	0.25	0.15	0.15	0.1
Cpx	0.16	0.15	0.19	0.130	0.18	0.15	0.30	0.20	0.1
Spinel	0.02	0.01	0.01	0.010	0.01	0.01	0.20	0.20	0.3
Garnet	0.05	0.09	0.05	0.055	0.08	0.02	0.20	0.30	0.4

	Best fit to:							Source	
	UBS enr.	UBS dep.	UBS necks		LBS enr.	LBS dep.	LBS necks		
REE	1	2	3	4	5	6	7	A (A*)	ENR
La	48.39	23.90	30.47	10.30	52.57	18.41	77.48	0.9204	1.8
Ce	96.51	54.09	65.21	25.05	106.86	42.27	142.21	2.3829	4.02
Nd	38.94	27.07	30.00	15.40	43.64	22.20	53.77	1.7758	2.49
Sm	8.14	6.16	6.74	4.18	9.06	5.28	10.96	0.5772	0.73
Eu	2.48	1.87	2.14	1.45	2.71	1.68	3.10	0.2184	0.24
Gd	7.32	5.49	6.52	4.75	7.87	5.07	9.38	0.7748	0.83
Dy	6.10	4.44	5.80	4.89	6.36	4.38	7.33	0.9581	0.85
Ho	1.13	0.78	1.12	1.02	1.14	0.81	1.45	0.2132	0.18
Er	2.65	1.75	2.76	2.75	2.63	1.89	3.58	0.624	0.49
Yb	2.10	1.39	2.22	2.38	1.90	1.41	2.42	0.6409 (0.5916)	0.42
Lu	0.30	0.20	0.31	0.34	0.27	0.20	0.31	0.0962 (0.0888)	0.06

enr.: more enriched lava from sequence.
dep.: more depleted lava from sequence.
Source and melt mineralogy are taken arbitrary, but similar to those used in other partial melting calculations (McKenzie and O'Nions, 1995; Mertz et al., 2001; Abdel-Rahmann, 2002). Modeling was performed using a spinel-garnet lherzolite mantle source assemblage with five different modes. All mantle phases are assumed to remain residual in the partial melted lherzolite, because none of them is melted out at degrees of melting ranging from 0.1% to 10%. Nos. 1 to 7 are calculated best fit melts produced by different batch partial melting degrees. The starting source mode, melt mode, degrees of melting and mantle source type used to produce each of the calculated melts are as follows.
Melt no. 1: source mode a, melt mode a, 1% melting of source A to produce more enriched lavas from UBS.
Melt no. 2: source mode a1, melt mode a, 4–5% melting of source A to produce more depleted lavas from UBS.
Melt nos. 3–4: source mode b, melt mode b, 2% and 8% melting of source A respectively to produce UBS necks.
Melt no. 5: source mode c, melt mode b, 1% melting of source A* to produce more enriched lavas from LBS.
Melt no. 6: source mode c1, melt mode b, 4% melting of source A* to produce more depleted lavas from LBS.
Melt no. 7: source mode d, melt mode c, 1.5% melting of source ENR to produce LBS basanitic necks.
Sources: A: 1.3 times primitive mantle of Sun and McDonough (1989); A*: 1.3 times primitive mantle of Sun and McDonough (1989), except Yb and Lu (1.2×); ENR: MORB source (McKenzie and O'Nions, 1995) enriched by 8% metasomatic melt, formed by extraction of 0.3% of fractional melting of MORB source.

Another factor that could produce these low element ratios is the assimilation of small amounts of pelagic sedimentation to the mantle source. On the Ce/Pb vs. Nb/U diagram (Fig. 12A), an intermediate UBS sample (FE01-36) plots far away from the field defined for OIB+MORB and is shifted towards the compositions of arc and continental crustal rocks, and of pelagic sediments from the Nazca plate. This kind of signature is also observed in other contemporaneous Patagonian Plateau Lavas (e.g. main-plateau lavas of Gorring and Kay, 2001; Fig. 12A). The presence of quartz xenocrysts in most UBS-intermediate lavas, together with isotopic signatures (see below) and incompatible elements patterns and ratios (Figs. 7, 8, 11 and 12A and B), favours the hypothesis of some crustal contamination and/or mingling, rather than the participation of pelagic sediments. Furthermore, an isotopic mixing curve between an asthenospheric source (N-MOR basalt from the Chile Ridge, from Guivel et al., 2003) and

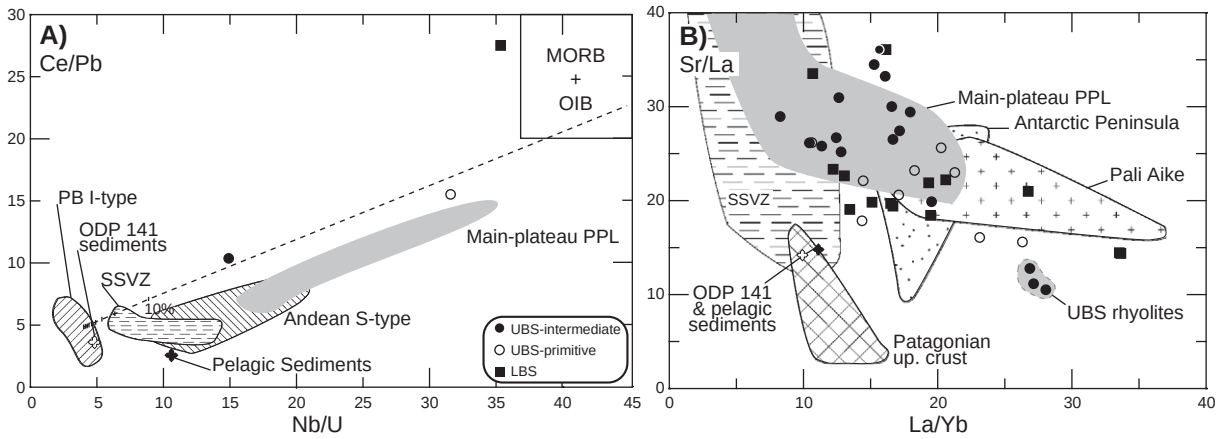

Fig. 12. Plots of (A) Ce/Pb vs. Nb/U and (B) Sr/La vs. La/Yb for MCC rocks showing that UBS-intermediate lavas (black filled circles) have ratios (low Ce/Pb, Nb/U and high Sr/La) indicating influence of some contaminant (crustal and/or arc-related) component. Ce/Pb vs. Nb/U ratio plot includes only ICP-MS data. Also shown mixing curve between N-MORB (Sun and McDonough, 1989) and Patagonian Batholith rocks (Kilian and Behrmann, 2003), tick every 10%. Field for OIB+MORB is from Klein and Karsten (1995). Data fields shown for comparison are: SSVZ (horizontal rules; Klein and Karsten, 1995), Patagonian upper crust (left diagonal rule: Andean S-type, right diagonal rule: PB I-type; Kilian and Behrmann, 2003), Chile Trench and pelagic Nazca plate sediments (open and filled cross, respectively, Kilian and Behrmann, 2003), and other slab window-related lavas: Pali-Aike (small crosses, D'Orazio et al., 2000), Antarctic Peninsula (fine stipple, Hole et al., 1995) and main-plateau Patagonian Plateau Lavas (grey field, Gorring and Kay, 2001).

a representative sample from Paso de las Llaves granite (Fig. 11, curve B) indicates that some interaction between the upwelling basaltic magmas and crustal anatectic products could have occurred, contributing to the contaminated signature of UBS-intermediate lavas.

Another important and distinctive characteristic of UBS-intermediate lavas is their high Sr/La ratio. These lavas (like SSVZ lavas) display higher Sr/La ratios than Patagonian crustal rocks and Chile Trench sediments (Fig. 12B), and therefore their signature cannot be accounted for crustal contamination. Alternatively, this signature could be ascribed to the involvement of slab-melts and/or arc magmas components in the genesis of these lavas (also with high La/Nb ratios and negative Nb–Ta and Ti anomalies, Fig. 8).

To check probable end-members for MCC basalt source, several mixing models were calculated and are shown in Fig. 11. Both LBS and UBS basalts fit mixing curve A between asthenospheric mantle (basalts from the Chile Ridge, from Guivel et al., 2003) and 70–80% of an enriched component (EM-I, from Zindler and Hart, 1986). Nevertheless, in order to explain relatively higher observed Sr isotopic values than those modelled for curve A, some crustal-derived component (such as Chile Trench sediments or the Patagonian Batholith) has to be involved in the genesis of these magmas (curves C and D, respectively; Fig. 11). The isotopic signature of the intermediate UBS basalt ($(^{87}Sr/^{86}Sr)_o$=0.70414 and εNd=+4.7) is also consistent with some upper crust participation as it falls close to the mixing curve between N-MORB and acid volcanic rocks from Jurassic–Cretaceous Ibáñez Formation (Fig. 11, curve E).

6.4. Geodynamic implications

The geochronological and geochemical constraints discussed above may be incorporated into a model based on the opening of two different slab windows beneath South America during Eocene and Pliocene, respectively (Fig. 13). This kind of model has already been proposed for different Patagonian basaltic sequences (Patagonian Plateau Lavas, Pali-Aike; Gorring et al., 1997, 2003, D'Orazio et al., 2000, 2001, respectively) during the Pliocene and Pleistocene–Recent, taking into account the temporal evolution of ridge–trench collision and slab window development under southern South America.

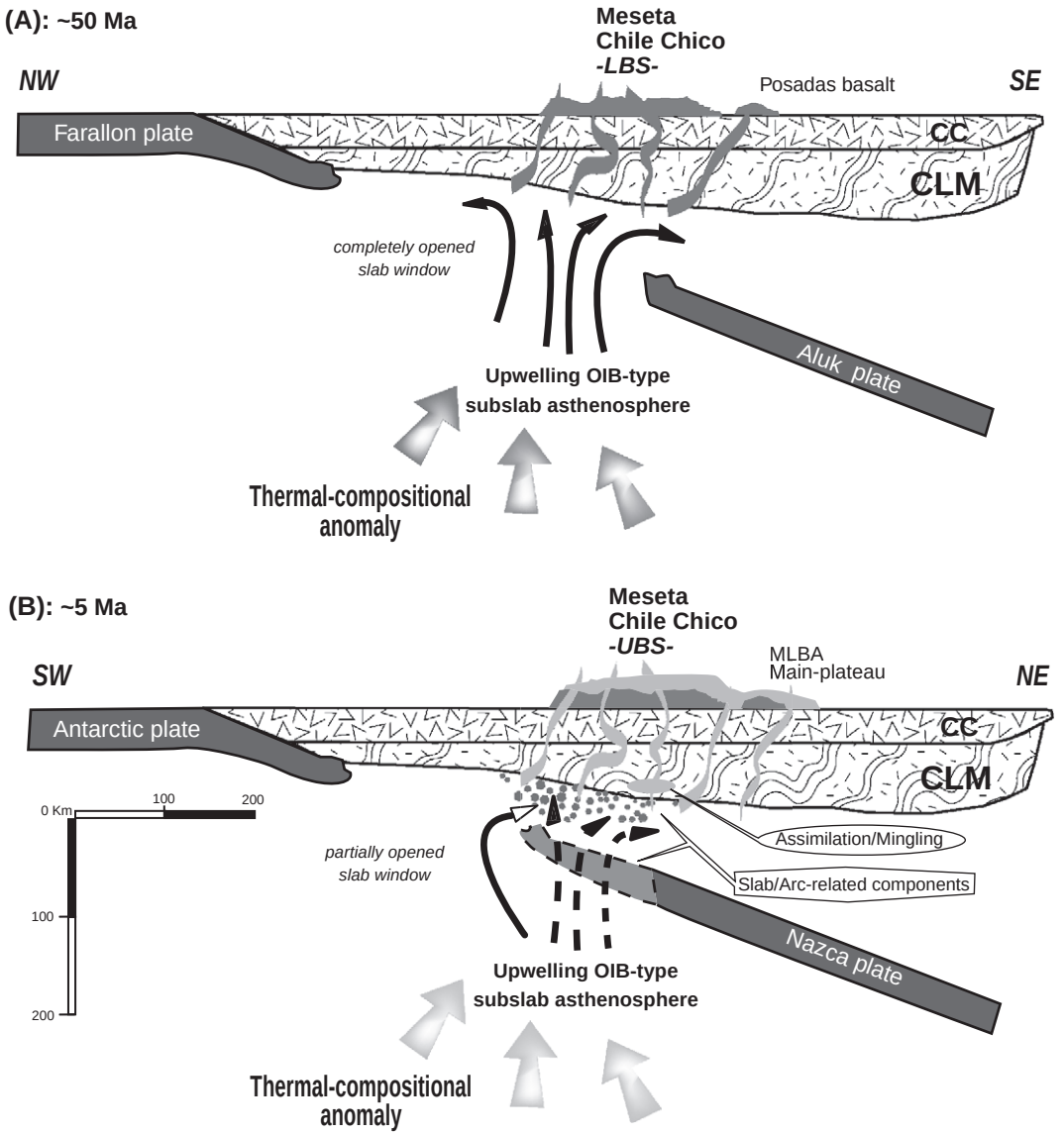

Fig. 13. (A) NW–SE cross-section of Patagonian Lithosphere during Eocene. At ~50 Ma, a slab window developed between Aluk and Farallon plates, formed due to their active ridge subduction (Cande and Leslie, 1986), was completely opened beneath the studied area. This setting together with the existence of a thermal and compositional anomaly under continental margin would produce the upwelling of an OIB-like subslab asthenosphere trough the slab window which would reach the surface uncontaminated. (B) SW–NE cross-section of Patagonian Lithosphere during Pliocene. At ~5 Ma, the slab window developed between Antarctic and Nazca plates due to the active Chile Ridge subduction (Cande and Leslie, 1986) was partially opened beneath the studied area. Again, the decompression of the mantle column under continental margin and the action of some (the same?) thermal and compositional anomaly under Patagonia would produce the upwelling of an OIB-like subslab asthenosphere trough the slab window. Some of these magmas (UBS-intermediate lavas) would interact with slab-derived and stored (underplated?) arc-related and/or crustal component, and others (UBS-primitive lavas) would not. CC: continental crust, CLM: continental? lithospheric mantle (modified from Gorring et al., 2003).

The proposed petrogenetic model for Mio–Pliocene basaltic magmatism in MCC is partly similar to the model presented by Gorring et al. (2003) for Plio–Pleistocene MLBA lavas (post-plateau lavas). Further, a slab window model for the Eocene magmatism, despite uncertainties about the geodynamic evolution, is strongly supported by the deep mantle, OIB-like geochemical signature, without continental contributions, of the Eocene lavas, and their similarity to other Eocene back-arc flood basalts which are also interpreted as slab window-related (Ramos and Kay, 1992; Kay et al., 2002). Petrogenetic modelling suggests an origin by low degrees of partial melting of primitive mantle source within the garnet-spinel stability field. These features, together with major element characteristics and the presence of spinel-lherzolite xenoliths in some LBS basalts (Espinoza and Morata, 2003a), indicate that rapid ascent of magmas through a thin continental crust occurred, and was accompanied by minor fractional crystallization and assimilation, during the development of the slab window (Fig. 13A). All these features point out to an extensional tectonic regime in the Patagonian back-arc domain during the Eocene (Fig. 13A), probably as a consequence of prelate Paleocene–early Eocene compressional tectonics (Suárez and De la Cruz, 2000a). The rather limited exposure of Eocene basalts in the Patagonian back-arc domain would be a result of the subsequent Neogene tectonics (Lagabrielle et al., 2004). The occurrence of highly enriched basanites during the later Eocene volcanism would be the result of melting of a metasomatically enriched MORB-like mantle source. As the Patagonian crust is relatively young (<0.5 Ga, Riccardi and Rolleri, 1980), the possibility for generation of enrichments like those of the basanites via crustal contamination is small, and their isotopic composition also indicate minor, if any, crustal participation in their genesis. Thus, the incompatible element enrichment could have been carried directly into the magma source by subduction-related fluids or melts (Maury et al., 1992). These rocks are the latest generated by the positive thermal anomaly related to the upwelling of hot asthenosphere passing through the window as it migrated southeastward, and represent the end of magmatism in the LGCBA region.

After a ~24 Ma long period of magmatic quiescence in this region, collision of successive segments of the active Chile Ridge with the partially sediment-filled Chile Trench would induce once more the development of a slab window beneath Patagonia. At ~13 Ma (Middle Miocene), just after the Chile Ridge subduction began near Tierra del Fuego (~15 Ma, ~55°S; Cande and Leslie, 1986), the first response to the changing tectonic regime is recorded in MCC with the early extrusion of UBS rhyolites, related with coeval plutonism in the region (Paso de las Llaves granite). This indicates that tectonic conditions needed for volcanism (abnormal stress regime, extensive structures) were already set up at this time and ready for the next mafic magmatism. The magmatism would have begun between 12 and 10 Ma, prior to the arrival of the slab window beneath the LGCBA region, but no rocks with this age have been found. We may speculate that these basalts would have had a MORB-like signature, since they would have been generated on the mantle wedge above young and hot subducted oceanic lithosphere. At ~7–8 Ma, a intense new magmatic event occurred, during which were emplaced UBS basalts, the first direct slab window-related lavas in this period. Though there is no age correlation between UBS-primitive and UBS-intermediate rocks, these early basalts have intermediate affinities (Table 5). Their Nb and Ti negative anomalies, along with high La/Sr and La/Nb ratios, low Ce/Pb and Nb/U ratios, Pb and Sr positive anomalies and more radiogenic isotopic values, suggest the contribution of slab/arc-derived and/or crustal components. Part of these components would be supplied by the leading edge of the Nazca plate before the complete opening of a slab window under LGCBA region. This kinematic pattern is consistent with the geotectonic model of Gorring et al. (1997), where at ~8 Ma the Nazca plate edge of the SCR segment, which subducted at ~12 Ma (SCR-2), was <100 km directly south of MCC (projected onto surface). The arc component in these lavas (high Sr/La) may be represented by materials stored at the base of the lithospheric mantle or mixed in the mantle wedge, or both. Around ~6 Ma, the SCR-1 segment collided with the continent at latitudes south of LGCBA region (Fig. 1B). The oblique subduction and the still ongoing divergence (Thorkelson, 1994, 1996) at the Chile Ridge axis initiated the development of a slab window under

MCC. At ~5 Ma, the partially opened slab window may have been located beneath the studied area (Fig. 13B). Consequently, as proposed for the Eocene period, together with a new extensional tectonic phase (as a consequence of late Miocene contractional tectonics, Ramos, 1989; Flint et al., 1994), decompressional melting would occur in the subslab asthenosphere, emplacing contaminated magmas (UBS-intermediate lavas, see above) plus some unaltered magmas (UBS-primitive lavas). Indeed, the Mio–Pliocene primitive magmas (like LBS lavas) show almost no evidence of slab/arc and crustal components (high Nb/U, Ce/Pb, low La/Nb; Figs. 7, 8, 11 and 12), and were likely quickly emplaced at the stage of full development of the slab window.

The Mio–Pliocene flood basaltic volcanism would have continued as long as the slab window passed below the LGCBA region eastward, covering the Eocene sequence at MCC and reaching further to the east (MLBA and Patagonian Plateau Lavas?; Fig. 13B). The slab window would have reached then its maximum aperture below MLBA (Fig. 1B), generating the primitive and relatively uncontaminated Plio–Pleistocene lavas described on top of the Meseta (post-plateau basalts of Gorring et al., 2003).

The data presented here can account for the occurrence of a long-lived magmatism in this region of Patagonia since Eocene to Pliocene, as a consequence of some kind of thermal and compositional anomaly under this sector of the continent, responsible for the input of primitive OIB-like asthenospheric melts. The collision of different active ridge segments during Eocene and Miocene would produce significant changes in the tectonic regime on the continental margin. The respective opening of slab windows beneath Patagonia would then allow the upwelling of voluminous primitive basaltic melts from the sub slab asthenosphere.

7. Conclusions

MCC represent the westernmost exposure of the Neogene Patagonian Plateau Lavas. The origins of its two alkaline basaltic sequences are related to the opening of two different slab windows beneath southern Patagonia at ~50 Ma and ~5 Ma, respectively. Most products have strong OIB-like signatures, with no major contamination, but part of the Miocene UBS lavas has geochemical features indicating the contribution of a slab/arc and/or crustal component. Variations in the intensity of the extension would control the extent of the participation of crustal components, the strong extension during Eocene times allowing for rapid escape of uncontaminated magmas, while weak extension during part of the Mio–Pliocene activity would lead to greater contamination. Results of partial melting (REE-) modelling indicate an origin by low degrees of partial melting from a primitive mantle source at depths within the garnet-spinel stability field (~65–70 km) for both sequences.

Acknowledgments

Field and analysis support was provided by the FONDECYT project no. 1000125 and ECOS-CONICYT project no. C01U01. This work also forms part of a geologic mapping project of the Servicio Nacional de Geología y Minería in collaboration with the Regional Government of the XI Region, Chile. The authors acknowledge helpful reviews by M.A. Parada and P. Comin-Chiaramonti. We also wish to thank Mr. Leonardo Zuñiga for his field assistance and Mr. Jaime Martínez (U. de Chile) and Felipe Llona (Sernageomin) for the chemical analyses.

Appendix A. Analytical procedures

A.1. K–Ar ages

Nineteen new K–Ar dates for MCC rocks (16 whole-rock ages and 2 biotite and 1 amphibole separate ages) display ages ranging from early Eocene to early Pliocene (Table 5). Fourteen of these data were obtained at the Geochronology Laboratory of the Servicio Nacional de Geología y Minería in Santiago, Chile. Mineral concentrates were obtained by heavy liquid and magnetic methods, usually from the 60–80# fraction. Argon was purified on Pyrex extraction lines and the radiogenic ^{40}Ar volumes were determined using

standard isotopic dilution technique on a mass spectrometer MS10S, with a total precision of 1–2%. Analyses of K were made on triplicates by atomic absorption technique with a 0.7–1.3% precision, depending on K content. Errors are given as 2 sigma (2σ) and the Steiger and Jäger (1977) decay constant is used. The other five K–Ar ages were obtained in the Geochronology Laboratory at the Universté de Bretagne Occidentale, Brest, France. After crushing and sieving, the 0.30–0.15 mm fraction was cleaned with distilled water and then retained for analytical procedures: (1) one aliquot was powdered in an agate grinder for K analysis by atomic absorption after HF chemical dissolution and (2) 0.3–0.15 mm fraction were used directly for argon isotopic analysis. Argon extraction was performed under high vacuum by induction heating of a molybdenum crucible. Extracted gases were cleaned on two titanium sponge furnaces and finally purified with two Al–Zr SAES getters. Isotopic composition of argon and concentrations of radiogenic ^{40}Ar were measured using a 180°-geometry stainless steel mass spectrometer equipped with a 642 Keithley amplifier. The isotopic dilution method was applied using a ^{38}Ar spike buried as ions in aluminum targets, following the procedure described by Bellon et al. (1981). Isotopic ages, listed with their respective characteristic parameters in Table 5, were calculated using the constant recommended by Steiger and Jäger (1977), and ±2σ errors are quoted following the equation of Mahood and Drake (1982).

A.2. Mineral chemistry

Mineral chemical analyses (Table 2) and scanning electron microscope images were carried out using a SEM-Probe CAMEBAX SU-30 in the Electronic Microscopy Laboratory at the Geology Department of the University of Chile. All elements were measured using X-ray wavelength-dispersion spectrometry (WDS), with a 15 kV accelerating voltage, a 2 μm beam, a beam current of 10 nA and a counting time of 10 s. The quantitative analysis was made using on-board software (CAMECA SX-50), ZAF correction. Depending upon the analysed rock and mineral composition, different standards certified by P&H Developments were used. The detection limit for the analysed elements is 0.1 wt.%.

A.3. Whole-rock chemistry

The geochemical analysis of 40 representative samples of Tertiary Meseta Chile Chico volcanic rocks (major and trace elements, Table 4) were carried out by inductively coupled plasma-atomic emission spectrometry (ICP-AES) at the Geology Department of the University of Chile (Perkin Elmer P-430), the Servicio Nacional de Geología y Minería Chemical Laboratory, Santiago, Chile, and at the University of Bretagne Occidental Chemical Laboratory, Brest, France, using procedure described by Cotten et al. (1995). In all cases, samples were finely ground in an agate grinder. International standards used for calibration test were BCR-2, AGV-2 and G-2 (UCH), and ACE, BEN, JB-2, PM-S and WS-E (UBO). Rb was measured by flame atomic emission spectroscopy at the SERNAGEOMIN and UBO laboratories. Relative standard deviations for UBO analyses are ±1% for SiO_2, ±2% for other major elements except P_2O_5 and MnO (±0.01%), and ±5% for trace elements. Detection limits were 0.1% for major elements, 2 ppm for Th and Nb, 1 ppm for Ba, Sr, Zr, Y, Cr, V, Ni, Co, Sc, Cu, Zn, Hf, La, Ce, Nd and Sm, 0.1 ppm for Eu, Gd, Dy, Ho, Er and Yb, and 0.05 ppm for Lu. Additionally, three selected samples (samples FE01-39B, FE01-13, FE01-36) were also analyzed by ICP-MS at the Centro de Instrumentación Científica of the University of Granada, Spain, on a Perkin Elmer SCIEX-ELAN 5000 mass spectrometer.

A.4. Sr–Nd isotope data

The Sr and Nd isotopic composition of four selected samples from Eocene and Mio–Pliocene MCC lavas (three basalts and one rhyolite) were measured at the Centro de Instrumentación Científica of the University of Granada, Spain (Table 6), using a Finnigan MAT 262 thermal ionization mass spectrometer (TIMS) with variable multicollector and RPQ. Normalization value used for Sr mass discrimination correction was $^{88}Sr/^{86}Sr=8.375209$ and the reproducibility for successive determinations of the NBS-987 dissolved standard and the WSE powder standards were better than 0.0007% (2σ) and 0.0026% (2σ), respectively. No age corrections were done for Sr isotopic ratios to maintain

concordance with literature data. For the Nd determinations, the normalization value for Nd mass discrimination correction was $^{146}Nd/^{144}Nd=0.7219$. The reproducibility calculated from successive measures of the La Jolla standard solution was better than 0.0014% (2σ) and better than 0.0016% (2σ) on the WSE powder standard. Initial isotopic ratios were calculated based on determined or assumed ages for each sample.

References

Abdel-Rahmann, A.M., 2002. Mesozoic volcanism in the Middle East: geochemical, isotopic and petrogenetic evolution of extension-related alkali basalts from central Lebanon. Geol. Mag. 139 (6), 621–640.

Ayers, J.C., Dittmer, S.K., Layne, G.D., 1997. Partitioning of elements between peridotite and H_2O at 2.0–3.0 GPa and 900°–1100°, and applications to models of subduction processes. Earth Planet. Sci. Lett. 150, 381–398.

Baker, P.E., Rea, W.J., Skarmeta, J., Caminos, R., Rex, D.C., 1981. Igneous history of the Andean Cordillera and Patagonian Plateau around latitude 46°S. Philos. Trans. R. Soc. Lond., A 303, 105–149.

Bellon, H., Quoc Buu, N., Chaumont, J., Philippet, J.C., 1981. Implantation ionique d'argon dans une celibe support: application au tracage isotopique d l'argon contenu dans les minéraux et les roches. C. R. Acad. Sci., Paris 292, 977–980.

Benoit, M., Aguillón-Robles, A., Calmus, T., Maury, R., Bellon, H., Cotten, J., Bourgois, J., Michaud, F., 2002. Geochemical diversity of late Miocene volcanism in Southern Baja California, Mexico: implications of mantle and crustal sources during the opening of an asthenospheric slab window. J. Geol. 110, 627–648.

Biddle, K., Uliana, R., Mitchum, R., Fitzgerald, M., Wright, R., 1986. The stratigraphic and structural evolution of the central and eastern Magallanes Basin, southern South America. In: Allen, P.A., Homewood, P. (Eds.), Foreland Basins, Special Publication of the International Association of Sedimentologists vol. 8, pp. 41–61.

Bourgois, J., Guivel, C., Lagabrielle, Y., Calmus, T., Boulègue, J., Daux, V., 2000. Glacial–interglacial trench supply variation, spreading-ridge subduction, and feedback controls on the Andean margin development at the Chile Triple Junction area (45–48°S). J. Geophys. Res. 105, 8355–8386.

Busteros, A., Lapido, O., 1983. Rocas básicas en la vertiente noroccidental de la meseta del Lago Buenos Aires, provincia de Santa Cruz. Rev. Asoc. Geol. Argent. 38 (3–4), 427–436.

Cande, S.C., Kent, D.V., 1992. A new geomagnetic polarity timescale for the late Cretaceous and Cenozoic. J. Geophys. Res. 97, 13917–13951.

Cande, S.C., Leslie, R.B., 1986. Late Cenozoic tectonics of the southern Chile Trench. J. Geophys. Res. 91, 471–496.

Cembrano, J., Lavenu, A., Reynolds, P., Arancibia, G., Lopez, G., Sanhueza, A., 2002. Late Cenozoic transpressional ductile deformation north of the Nazca–South America–Antarctica triple junction. Tectonophysics 354, 289–314.

Charrier, R., Linares, E., Niemeyer, H., Skarmeta, J., 1979. K–Ar ages of basalt flows of the Meseta Buenos Aires in southern Chile and their relation to the southeast Pacific triple junction. Geology 7, 436–439.

Cotten, J., Le Dez, A., Bau, M., Caroff, M., Maury, R.C., Dulski, P., Fourcade, S., Bohn, M., Brousse, R., 1995. Origin of anomalous rare-earth elements and ytrium enrichments in subaereally exposed basalts: evidence from French Polynesia. Chem. Geol. 119, 115–138.

DeMets, C., Gordon, R.G., Argus, D.F., Stein, S., 1990. Current plate motions. Geophys. J. Int. 101, 425–478.

D'Orazio, M., Agostini, S., Mazzarini, F., Innocenti, F., Manetti, P., Haller, M., Lahsen, A., 2000. The Pali Aike Volcanic Field, Patagonia: slab-window magmatism near the tip of South America. Tectonophysics 321, 407–427.

D'Orazio, M., Agostini, S., Innocenti, F., Haller, M.J., Manetti, P., Mazzarini, F., 2001. Slab window-related magmatism from southernmost South America: the late Miocene mafic volcanics from the Estancia Glencross Area (~52°S Argentina–Chile). Lithos 57, 67–89.

Demant, A., Hervé, F., Pankhurst, R., Suárez, M., 1996. Geochemistry of early Tertiary back-arc basalts from Aysén, southern Chile (44–46°S): geodynamic implications. Third ISAG, St Malo, pp. 17–19.

Dickinson, W.R., 1997. Tectonic implications of Cenozoic volcanism in coastal California. Geol. Soc. Amer. Bull. 109, 936–954.

Dickinson, W.R., Snyder, W.S., 1979. Geometry of subducted slabs related to San Andreas transform. J. Geol. 87, 609–627.

Elliot, T., Plank, T., Zindler, A., White, W., Bourdon, B., 1997. Element transport from slab to volcanic front at the Mariana arc. J. Geophys. Res. 102, 14991–15019.

Espinoza, F., 2003. Petrología y Geoquímica de los Basaltos Cenozoicos de la meseta Chile Chico, 46°35′–46°47′S–71°46′–72°02′W, XI Región de Aysén, Chile. MSc thesis. Departamento de Geología, Universidad de Chile, Santiago.

Espinoza, F., Morata, D., 2003a. Xenolitos mantelicos incluidos en Cerro Lápiz, meseta Chile Chico, XI Región de Aysén, Chile. X Congreso Geológico Chileno, Concepción.

Espinoza, F., Morata, D., 2003b. Petrogenesis de los basaltos cenozoicos de la Meseta Chile Chico, XI Región de Aysén, Chile. X Congreso Geológico Chileno, Concepción.

Espinoza, F., Morata, D., Suárez, M., De la Cruz, R., 2003. The meseta Chile Chico basalts, eastern central Patagonian Cordillera: K–Ar geochronology and geochemistry of a compresional to extensional back-arc volcanism. IV South American Symposium on Isotope Geology, Salvador, Brazil.

Flint, S.S., Prior, D.J., Agar, S.M., Turner, P., 1994. Stratigraphic and structural evolution of the Tertiary Cosmelli Basin and its relationship to the Chile Triple Junction. J. Geol. Soc. (Lond.) 151, 251–268.

Flynn, J.J, Novacek, M., Dodson, H., Frassinetti, D., McKenna, M., Norell, M., Sears, K., Swisher III, C., Wyss, A., 2002. A new fossil mammal assemblage from the southern Chilean Andes:

implications for geology, geochronology, and tectonics. J. South Am. Sci. 15, 285–302.

Frassinetti, D., Covacevich, V., 1999. Fauna de invertebrados fósiles marinos de la Formación Guadal en Pampa Castillo, sur del lago General Carrera, Aysén, Chile. Servicio Nacional de Geología y Minería, Chile, p. 51.

Gorring, M., Kay, S., 2001. Mantle processes and sources of Neogene slab window magmas from southern Patagonia, Argentina. J. Petrol. 42 (6), 1067–1094.

Gorring, M., Kay, S., Zeitler, P., Ramos, V., Rubiolo, D., Fernández, M., Panza, J., 1997. Neogene Patagonian Plateau Lavas: continental magmas associated with ridge collision at the Chile Triple Junction. Tectonics 16 (1), 1–17.

Gorring, M., Singer, B., Gowers, J., Kay, S.M., 2003. Plio–Pleistocene basalts from the Meseta del Lago Buenos Aires, Argentina: evidence for asthenosphere–lithosphere interactions during slab window magmatism. Chem. Geol. 193, 215–235.

Gripp, A.E., Gordon, R.G., 1990. Current plate velocities relative to the hotspots incorporating the NUVEL-1 global plate motion model. Geophys. Res. Lett. 17, 1109–1112.

Guivel, C., Lagabrielle, Y., Bourgois, J., Maury, R.C., Fourcade, S., Martin, H., Arnaud, N., 1999. New geochemical constraints for the origin of ridge-subduction-related plutonic and volcanic suites from the Chile Triple Junction (Taitao Peninsula and Site 862, LEG ODP on the Taitao Ridge). Tectonophysics 311, 83–111.

Guivel, C., Lagabrielle, Y., Bourgois, J., Martin, H., Arnaud, N., Fourcade, S., Cotton, J., Maury, R.C., 2003. Very shallow melting of oceanic crust during spreading ridge subduction: origin of near-trench quaternary volcanism at the Chile Triple Junction. J. Geophys. Res. 108 (B7), 2345.

Hawkesworth, C.J., Norry, M.J., Roddick, J.C., Baker, P.E., Francis, P.W., Thorpe, R.S., 1979. $^{143}Nd/^{144}Nd$, $^{87}Sr/^{86}Sr$ and incompatible element variations in calk-alkaline andesites and plateau lavas from South America. Earth Planet. Sci. Lett. 42, 45–57.

Hawkesworth, C.J., Turner, S., Peate, D., McDermott, F., van Calsteren, P., 1997. Elemental U and Th variations in island arc rocks: implications for U-series isotopes. Chem. Geol. 139, 207–221.

Hole, M.J., Saunders, A.D., Rogers, G., Sykes, M.A., 1995. The relationship between alkaline magmatism, lithospheric extension and slab window formation along continental destructive plate margins. In: Smellie, J.L. (Ed.), Volcanism Associated with Extension at Consuming Plate Margins, Special Publication-Geological Society of London, vol. 81, pp. 265–285.

Irvine, T.N., Baragar, W.R.A., 1971. A guide to the chemical classification of the common volcanic rocks. Can. J. Earth Sci. 8, 523–548.

Kay, S.M., Ramos, V.A., Márquez, M., 1993. Evidence in Cerro Pampa volcanic rocks for slab-melting prior to ridge collision in southern South America. J. Geol. 101, 703–714.

Kay, S.M., Ramos, V.A., Gorring, M.L., 2002. Geochemistry of Eocene plateau basalts related to ridge collision in southern Patagonia. XV Congreso Geológico Argentino, El Calafate.

Kilian, R., Behrmann, J., 2003. Geochemical constraints on the sources of southern Chile Trench sediments and their recycling in arc magmas of the Southern Andes. J. Geol. Soc. (Lond.) 160, 57–70.

Klein, E.M., Karsten, J.L., 1995. Ocean ridge basalts with convergent margin geochemical affinities from the southern Chile Ridge. Nature 374, 52–57.

Lagabrielle, Y., Suárez, M., Rosselló, E.A., Hérail, G., Martinod, J., Régnier, M., de la Cruz, R., 2004. Neogene to quaternary tectonic evolution of the Patagonian Andes at the latitude of the Chile Triple Junction. Tectonophysics 385, 211–241.

La Tourrette, T.Z., Kennedy, A.K., Wasserburg, G.J., 1993. Thorium–uranium fractionation by garnet: evidence for a deep source and rapid rise of ocean basalts. Science 261, 739–742.

Le Maitre, R.W., Bateman, P., Dudek, A., Keller, J., Lameyre Le Bas, M.J., Sabine, P.A., Schmid, R., Sorensen, H., Streckeisen, A., Wolley, A.R., Zanettin, B., 1989. A Classification of Igneous Rocks and Glossary of Terms. Blackwell, Oxford.

Mahood, G.A., Drake, R.E., 1982. K–Ar dating young rhyolitic rocks: a case study of the Sierra La Primavera, Jalisco, Mexico. Geol. Soc. Amer. Bull. 93, 1232–1241.

Marshall, L.G., Salinas, P., 1990. Stratigraphy of the Río Frías Formation (Miocene), along the Alto Río Cisnes, Aysén, Chile. Rev. Geol. Chile 17, 57–88.

Maury, R.C., Defant, C., Joron, M.J., 1992. Metasomatism of the sub-arc mantle inferred from trace elements in Philippine xenoliths. Nature 360, 661.

McKenzie, D., O'Nions, R.K., 1995. The source regions of oceanic island basalts. J. Petrol. 36, 133–159.

Mertz, D.F., Weinrich, A., Sharp, W.D., Renne, P.R., 2001. Alkaline intrusions in a near-trench setting, Franciscan complex, California: constraints from geochemistry, petrology and $^{40}Ar/^{39}Ar$ chronology. Am. J. Sci. 301, 877–911.

Morimoto, N., Fabries, J., Ferguson, A.K., Ginzburg, I.V., Ross, M., Seifert, F.A., Zussmann, J., Aoki, K., Gottardi, G., 1988. Nomenclature of piroxenes. Am. Mineral. 173, 1123–1133.

Nakamura, N., 1974. Determination of REE, Ba, Fe, Mg, Na and K in carbonaceous and ordinary chondrites. Geochim. Cosmochim. Acta 38, 757–775.

Nicholson, H., Latin, D., 1992. Olivine tholeiites from Krafla, Iceland: evidence for variations in the melt fraction within a plume. J. Petrol. 33, 1105–1124.

Niemeyer, H., 1975. Geología regional del territorio comprendido entre el lago General Carrera y el río Chacabuco, Provincia de Aysén, Chile. Departamento de Geología, Universidad de Chile, Santiago.

Niemeyer, H., Skarmeta, J., Fuenzalida, R., Espinosa, W., 1984. Hojas Península de Taitao y Puerto Aysén, 1:500.000, N° 60–61. Servicio Nacional de Geología y Minería, Chile.

Niu, Y., Hékinian, R., 1997. Basaltic liquids and harzburgitic residues in the Garrett transform: a case study at fast spreading ridges. Earth Planet. Sci. Lett. 146, 243–258.

Pankhurst, R., Leat, P.T., Sruoga, P., Rapela, C., Márquez, M., Storey, B., Riley, T., 1998. The Chon Aike silicic Igneous Province of Patagonia and related rocks in West Antartica: a silicic LIP. J. Volcanol. Geotherm. Res. 81, 113–136.

Pankhurst, R., Weaver, S., Hervé, F., Larrondo, P., 1999. Mesozoic–Cenozoic evolution of the North Patagonian Batholith in Aysén, southern Chile. J. Geol. Soc. (Lond.) 156, 673–694.

Parada, M.A., Lahsen, A., y Palacios, C., 2001. Ages and geochemistry of Mesozoic–Eocene back-arc volcanic rocks in the Aysén region of the Patagonian Andes, Chile. Rev. Geol. Chile 28 (1), 25–46.

Pardo-Casas, F., Molnar, P., 1987. Relative motion of the Nazca (Farallón) and South American Plates since late Cretaceous time. Tectonics 6, 233–248.

Peccerillo, R., Taylor, S.R., 1976. Geochemistry of Eocene calk-alkaline volcanic rocks from the Kastamonu area, northern Turkey. Contrib. Mineral. Petrol. 58, 63–81.

Petford, N., Turner, P., 1996. Reconnaissance ^{40}Ar–^{39}Ar age and paleomagnetic study of igneous rocks around Coyhaique, S. Chile. Third ISAG, St Malo, France, pp. 625–627.

Petford, N., Cheadle, M., Brewer, T., Barreiro, B., 1996. Age and Origin of Southern Patagonian Flood Basalts, Chile Chico Region (46°45′S). Third ISAG, St Malo, France, pp. 629–632.

Ramos, V.A., 1989. Andean foothills structures in Northern Magallanes Basin, Argentina. Am. Assoc. Pet. Geol. Bull. 73, 887–903.

Ramos, V.A., Kay, S.M., 1992. Southern Patagonian Plateau basalts and deformation: backarc testimony of ridge collision. Tectonophysics 205, 261–282.

Riccardi, A.C., 1988. The Cretaceous system of southern South America. Geol. Soc. Am., 168.

Riccardi, A.C., Rolleri, E.O., 1980. Cordillera Patagónica Austral. Segundo Simp. Geo. Reg. Argent. 2, 1173–1306.

Shaw, D.M., 1970. Trace elements fractionation during anatexis. Geochim. Cosmochim. Acta 34, 237–243.

Simonetti, A., Shore, M., Bell, K., 1996. Diopside phenocrysts from nephelinite lavas, Napak volcano, eastern Uganda: evidence for magma mixing. Can. Mineral. 34, 411–421.

Steiger, R.H., Jäger, E., 1977. Subcommission on geocronology: convention and the use of decay constant in geo- and cosmochronology. Earth Planet. Sci. Lett. 36, 359–362.

Stern, C.R., Kilian, R., 1996. Role of the subducted slab, mantle wedge and continental crust in the generation of adakites from the Andean Austral Volcanic Zone. Contrib. Mineral. Petrol. 123, 263–281.

Stern, C.R., Frey, F.A., Futa, K., Zartman, R.E., Peng, Z., Kyser, T.K., 1990. Trace-element and Sr, Nd, Pb and O isotopic composition of Pliocene and Quaternary basalts of the Patagonian Plateau Lavas of southernmost South America. Contrib. Mineral. Petrol. 104, 294–308.

Suárez, M., De la Cruz, R., 2000a. Tectonics in the eastern–central Patagonian Cordillera (45°30′–47°30′S). J. Geol. Soc. (Lond.) 157 (5), 995–1001.

Suárez, M., De la Cruz, R., 2000b. Geología de la zona del lago General Carrera, Región de Aysén, Chile. IX Congreso Geológico Chileno, Actas vol. 2, pp. 264–268.

Suárez, M., De la Cruz, R., 2001. Jurassic to Miocene K–Ar dates from eastern central Patagonian Cordillera plutonism, Chile (45°–48°S). Geol. Mag. 138 (1), 53–66.

Suárez, M., Demant, A., De la Cruz, R., 1999. Volcanismo calcoalcalino en W provincia Chon Aike: Grupo Ibañez, Jurásico Superior-Cretácico Inferior temprano, Cordillera Patagónica de Aysén, Chile (45°30′–46°30′S). IV Congreso Geológico Argentino, Salta, Actas, vol. II, pp. 186–189.

Suárez, M., De la Cruz, R., Troncoso, A., 2000. Tropical/subtropical upper Paleocene–lower Eocene fluvial deposits in eastern central Patagonia, Chile (46°45′). J. South Am. Earth Sci. 13 (6), 527–536.

Sun, S., McDonough, W.F., 1989. Chemical and isotopic systematics of oceanic basalts; implications for mantle composition and processes. In: Saunders, A.D, Norry, J.M. (Eds.), Magmatism in the Ocean Basins, Special Pub.-Geological Society of London vol. 42, pp. 313–345.

Thompson, R.N., Morrison, M.A., Hendry, G.L., Parry, S.J., 1984. An assessment of the relative roles of crust and mantle in magma genesis: an element approach. Philos. Trans. R. Soc., Lond., A 310, 549–590.

Thomson, S.N., Hervé, F., Stöckhert, B., 2001. Mesozoic–Cenozoic denudation history of the Patagonian Andes (southern Chile) and its correlation to different subduction processes. Tectonics 20, 693–711.

Thorkelson, D.J., 1994. Ridge subduction: kinematics and implications for the nature of mantle upwelling: discussion. Can. J. Earth Sci. 31, 1486–1489.

Thorkelson, D.J., 1996. Subduction of diverging plates and the principles of slab window formation. Tectonophysics 255, 47–63.

Vargas, G., Hervé, F., 1995. Emplazamiento hipabisal Mioceno tardío del stock de Paso de las Llaves en la región de tras arco, Aysén. Comun.-Dep. Geol., Univ. Chile, Santiago 46, 3–16.

Wittke, J.H., Mack, L.E., 1993. OIB-like mantle source for continental alkaline rocks of the Balcones province, Texas: trace elements and isotopic evidence. J. Geol. 101, 333–344.

Zindler, A., Hart, S., 1986. Chemical geodynamics. Annu. Rev. Earth Planet Sci. 14, 493–571.